Moisture Fluxes over the Alps

Master's Thesis

Faculty of Science
University of Bern

presented by

Donatus Berger

2014

Supervisor:
Prof. Dr. Olivia Romppainen-Martius

Institute of Geography and
Oeschger Centre for Climate Change Research, University of Bern

Advisor:
Paul Froidevaux

Institute of Geography and
Oeschger Centre for Climate Change Research, University of Bern

Abstract

The amount of precipitation is crucial for the Alpine region because it is a region which is highly sensitive to floods due to the presence of numerous rivers and lakes. Moisture fluxes are an important factor for the amount of precipitation that can be triggered by orographic precipitation. This study focuses on the investigation of the integrated vapour transport (IVT) for three northern (Prealps, Eastern Switzerland, Jura) and two southern (Valais, Ticino) Alpine regions. The northern and southern Alpine regions differ in the direction from where the most intense IVTs originate from. The most intense IVT are found to come from the South-West, West and North-East for northern Alpine regions whereas the most intense IVTs for southern Alpine regions originate from the West, South-West and South. Regarding the seasonality, the most intense IVTs occur in summer and autumn. The interannual variability of IVT varies between plus and minus 10-15% around the long-term mean. This variability is mainly explained by the variation of the steering wind. Wavelet analyses show that IVT exhibits a periodicity between 5 and 8 years during the second half of the 20th century. Furthermore, a periodicity at lower freuquencies, namely at more than 36 years, is detected for IVT. In all predefined regions, trend analyses reveal non-significant negative trends of IVT. However, trends of IVT are positive and partly statistically significant in the South-East of the Alpine area. All regions exhibt negative trends of steering wind and positive trends of total precipitable water (TPW). The trends are stronger for steering wind than for TPW and thus determine the negative trends of IVT.

Contents

Chapter 1

Introduction

1.1 Motivation

Water is a very important resource in the ecological system of the Earth. On the Earth's surface, it can be transported in little mountain streams up to giant rivers as the Amazon River with a mean discharge of about 200,000 $m^3\,s^{-1}$ (Oki and Kanae, 2006). However, water can evaporate and thus it is also transported in the atmosphere as water vapour and varies the local moisture content of air. This variability of moisture content of air varies also the amount of precipitation as the relative moisture content is a key factor for the triggering of precipitation (e.g. Panziera and Germann, 2010). The amount of precipitation in the Alpine region, especially in Switzerland, is crucial because it is a region which is highly sensitive to floods due to the presence of numerous rivers and lakes.

It is known that floods are a major threat for Alpine areas beacause they cause considerable economic impacts on society (Hilker et al., 2009). Recent floods in the Swiss Alps, such as the the events in August 2005, August 2007, October 2011 and June 2013, prove this hazard (Stucki et al., 2012; FOEN, 2008, 2014). In the case of the floods in October 2011, not only heavy precipitation caused the floods but also rising temperatures, which led to the melting of large quantities of snow that had fallen some days before (FOEN, 2014; Rössler et al., 2014). While there are numerous causes leading to this flood in October 2011 (fresh snow, rise of snow line, local enhancement of precipitation, moist neutral and saturated layer rising above a cold, blocked layer), one paramter was particularly important and probably constitutes the backbone of the flood: an exceptional amount of moisture was transported towards the Alpine ridge.

As mentioned beforehand, the moisture content of the air presents an essential part in the overall system of triggering precipitation and floods beside other factors. The momentous role of moisture serves as motivation of this study to investigate the mois-

ture fluxes over the Alps. The investigation of moisture fluxes bears the advantage that not only the moisture content is taken into account but also the wind speed and wind direction. Thus, it is possible to quantify the advection of moisture towards a certain region and to determine the direction from where the moisture comes.

1.2 State of research

An important term related to moisture fluxes are atmospheric rivers. Atmospheric rivers are narrow filaments of enhanced moisture transport in the lower troposphere and convey the majority of the poleward moisture transport (Ralph and Dettinger, 2011; Lavers et al., 2012; Lavers and Villarini, 2013). Atmospheric rivers are of particular importance in coastal regions because heavy precipitation can occur when they make landfall, possibly leading to floods (Lavers et al., 2012). Many studies have shown the relation between atmopheric rivers and floods, for example in western North America (Ralph et al., 2006; Neiman et al., 2011) or the British Isles (Lavers et al., 2011, 2012). Lavers and Villarini (2013) show that atmospheric rivers can cause extreme precipitation in Europe also far inland up to the Alpine area, especially in the winter half-year.

During winter the Alpine precipitation is dominated mainly by North Atlantic moisture source (Sodemann and Zubler, 2010). In contrast, a continental mode exists during summer, with a remarkable contribution of moisture from Central European land areas (Sodemann and Zubler, 2010). This shows that moisture sources for Alpine precipitation undergo a strong seasonal cycle (Sodemann and Zubler, 2010). Furthermore, Sodemann and Zubler (2010) found clear differences between the Northern Alps and Southern Alps. The Northern Alps receive most of the moisture from the North Atlantic Ocean and the Central European land sources. On the other hand, the southern Alpine moisture sources originate predominantly from the Mediterranean. This last point is supported by the fact that 73% of the heavy precipitation events in the Southern Alps are associated with a PV-streamer (Martius et al., 2006). PV-streamers induce a strong southerly flow ahead of the forward flank of the streamer, which leads to a strong moisture flux from the Mediterranean towards the Alps.

Another important point is the evolution of the moisture content of the air in the future. It is generally agreed that the future moisture content of the air will increase as the atmosphere is able to take up around 7% more moisture per Kelvin warming according to the Clausius-Clayperon relation (e.g., Held and Soden, 2006). Thus, the potential for more intense heavy precipitation will increase. Observations over the last decades show an already increasing freqency of heavy precipitation events in winter (CH2011, 2011). However, studies show that the positive trends of column-integrated water vapour are not evident over Europe (Trenberth et al., 2005; Ross and Elliott,

2001). These findings reveal the problem that the regional response to climate change is very complex and highly nonlinear due to different feedback mechanisms. The Swiss Climate Change Scenarios CH2011 (2011) identify the following main uncertainties for heavy precipitation predictions: large-scale circulation changes, precipitation processes and convection, role of soil moisture.

1.3 Objectives of the study

Previous studies have assessed the relevance of atmospheric rivers for the moisture transport in the extratropics. Furthermore, moisture sources for Alpine precipitation have been investigated as well as the role of moisutre fluxes on the triggering of heavy precipitation, possibly leading to flood events. However, the missing investigations of the climatological characteristics and the temporal variability of moisture fluxes over the Alps constitute a gap of knowledge in this field of research. This thesis aims at filling this gap, by performing climatological and time series analyses of moisture fluxes over the Alpine region. Thus, the following tasks are addressed:

- Perform climatological analyses of moisture fluxes, including the following questions:
  - Where do most of the moisture fluxes come from?
  - Where do the most intense moisture fluxes come from?
  - What is the seasonal cycle of moisture fluxes and which factors determine this cycle?
  - What is the vertical profile of moisture fluxes?
- Analyse the temporal variability of moisture fluxes, including the following questions:
  - How strong is the interannual variablity of moisture fluxes?
  - Are there any periodicities in moisture fluxes?
  - Do the moisture fluxes exhibit any trends?

Chapter 2

Data

This chapter gives an overview of the data used in the analyses. First, the atmospheric reanalysis data sets are described. Second, the radio sounding data from Payerne are presented.

2.1 Atmospheric reanalysis data

Atmospheric reanalysis data combine numerical weather prediction models with observations (Dee et al., 2014). This combination results in a better estimation of the state of the atmosphere over a defined time period which is suitable for climatological studies. It bears the advantage of globally gridded data with a high temporal resolution while simulataneously taking into account measured data with a certain assimilation scheme.

2.1.1 ERA-Interim reanalysis

The ERA-Interim (Dee et al., 2011) data set is the latest global reanalysis provided by the European Centre for Medium-Range Weather Forecasts (ECMWF). It has a horizontal spatial resolution of 0.75° x 0.75° longitude and latitude respectively which is interpolated to a 1° by 1° grid. ERA-Interim consists of 60 model levels and features a 6-hourly time resoultion. The data set covers the time period from 1 January 1979 to present, but the data is extended continuously.

2.1.2 Twentieth Century Reanalyis (20CR)

The 20CR (Compo et al., 2011) data set is also a global reanalysis. It is produced by the National Oceanic and Atmospheric Administration (NOAA) in collaboration with

the Cooperative Institute for Research in Environmental Sciences (CIRES). The horizontal resolution of the data is coarser compared to ERA-Interim. It has a horizontal resolution of 2° x 2° longitude and latitude respectively. The 20CR features a vertical resolution of 28 pressure levels and a 6-hourly time resolution. Compared to ERA-Interim, the 20CR covers a much longer time period, which goes from 1 January 1871 to 31 December 2010.

2.2 Radio sounding data

The radio sounding data are provided by the Federal Office of Meteorology and Climatology MeteoSwiss. Nowadays, a balloon with a radiosonde is launched twice a day (00 and 12 UTC) from Payerne. The radiosonde measures temperature, humidity, pressure and wind components.

Chapter 3

Methods

The methods chapter presents main definitions and analysis techniques that were used in this study. In addition, the defined regions are presented at the end of this chapter.

3.1 Definitions

First, the moisture flux is presented through the definition of both the horizontal moisture flux and the vertically integrated horizontal moisture flux. Then, the total precipitable water and the steering wind are defined.

3.1.1 Horizontal moisture flux

Equation 3.1 depicts the calculation of the horizontal moisture flux (MF [kg m^{-2} s^{-1}]) at different pressure levels.

$$\mathrm{MF} = \rho \sqrt{(qu)^2 + (qv)^2} \ \left[\mathrm{kg\ m^{-2}\ s^{-1}}\right] \tag{3.1}$$

q is the specific humidity in kg/kg, u and v are the zonal and meridional wind component in m s^{-1} respectively. ρ describes the density and is calculated as follows:

$$\rho = \frac{p}{T_v R_s} \ \left[\mathrm{kg\ m^{-3}}\right] \tag{3.2}$$

where p is the pressure in Pa, R_s is the specific gas constant for dry air (287.058 J $kg^{-1}K^{-1}$). T_v stands for the virtual temperature and is calculated as in equation 3.3.

$$T_v = T \left(1 + \left(\frac{1}{\varepsilon} - 1\right) q\right) \ \left[\mathrm{K}\right] \tag{3.3}$$

$$\varepsilon = \frac{M_{WV}}{M_{DA}} \tag{3.4}$$

Where ε is the molar mass ratio of water vapour ($M_{WV} \approx 18,01\,\mathrm{g\,mol^{-1}}$) and dry air ($M_{DA} \approx 28,97\,\mathrm{g\,mol^{-1}}$) and q is the specific humidity in kg/kg.

3.1.2 Vertically integrated horizontal moisture flux

Equation 3.5 shows how the vertically integrated horizontal moisture flux (hereafter IVT [$\mathrm{kg\,m^{-1}s^{-1}}$], integrated vapour transport) is calculated from the surface to 0.1 hPa for ERA-Interim and to 10 hPa for 20CR respectively (e.g., Neiman et al., 2008; Lavers and Villarini, 2013):

$$\mathrm{IVT} = \sqrt{\left(\frac{1}{g}\int_{surf}^{top} qu\,\mathrm{d}p\right)^2 + \left(\frac{1}{g}\int_{surf}^{top} qv\,\mathrm{d}p\right)^2}\ \left[\mathrm{kg\,m^{-1}s^{-1}}\right] \tag{3.5}$$

where g is the acceleration due to gravity, q is the specific humidity in kg/kg, u and v are the zonal and meridional wind in $\mathrm{m\,s^{-1}}$ respectively and $\mathrm{d}p$ is the pressure difference between two pressure levels.

3.1.3 Total precipitable water

The total precipitatable water (TPW [$\mathrm{kg\,m^{-2}}$]) is calculated as in equation 3.6. It shows that specific humidity is integrated over the whole column of atmosphere. It is called the TPW because it amounts the precipitation which would fall if all the moisture in the atmosphere condensated.

$$\mathrm{TPW} = \frac{1}{g}\int_{surf}^{top} \left(q + q_{ice} + q_{liquid}\right)\,\mathrm{d}p\ \left[\mathrm{kg\,m^{-2}}\right] \tag{3.6}$$

g is the acceleration due to gravity, q is the specific humidity in kg/kg including ice clouds q_{ice} and liquid q_{liquid} and $\mathrm{d}p$ is the pressure difference between two pressure levels.

3.1.4 Steering wind

In analogy to storm dynamics, the steering wind is calculated as the quotient of the IVT and the TPW (eq. 3.7). This is the wind profile averaged vertically and weighted by the amount of transported moisture.

$$\text{steering wind} = \frac{\mathrm{IVT}}{\mathrm{TPW}}\ \left[\mathrm{m\,s^{-1}}\right] \tag{3.7}$$

3.2 Analysis techniques

In this section, key analysis techniques that are used for the evaluations are presented and described.

3.2.1 Boxplots

In this study, all boxplots feature the same structure. The black bold horizontal line represents the median and the box around the median illustrates the interquartile range (IQR). Thus, this box always includes 50% of the data. The end of the whiskers are limited by the lowest and highest value still within the 1.5 IQR of the lower ($q_{0.25}$) and upper ($q_{0.75}$) quartile. These whiskers include 99.3% of the data in a normal distribution. The data outside of these whiskers are illustrated as circles and are called outliers.

3.2.2 Wavelet analysis

A wavelet analysis technique is used to identify if a time series oscillates with a certain periodicity (e.g., Welker and Martius, 2013). The anaylses are carried out using the R package *biwavelet*, which is a port of the softwares written by Torrence and Compo (1998) and Grinsted et al. (2004). The continuous wavelet transforms (CWTs) are computed based on the Morlet wavelet function (Torrence and Compo, 1998). The so-called cone of influence (COI) denotes the region of the CWT power spectrum in which edge effects become important (Torrence and Compo, 1998). The statistical significance of wavelet power is tested as follows: a peak in the wavelet power spectrum is significantly true if it is above the signal which is produced by a stationary process with a given mean power spectrum (Grinsted et al., 2004; Torrence and Compo, 1998). The time series are assumed to be approximately normally distributed with red noise characteristics.

3.2.3 Trend analysis

The trend analysis is used to investigate if the time series of the IVT, TPW and steering wind exhibit a trend for the time period of the datasets (ERA-Interim, 20CR). The trends are calculated with a linear regression using least squares estimation. This study uses R packages from Christoph Frei[1], where the trend estimations with linear regression are integrated.

[1] Available online on the lecture homepage of Analaysis of Climate and Weather Data: http://www.iac.ethz.ch/edu/courses/master/electives/acwd (last access on 4 August 2014).

3.3 Defined regions

Different Swiss regions are defined for the climatological analyses of moisture fluxes. To analyse the regions, the data are selected at the ERA-Interim and 20CR grid point closest to the predefined region respectively. We try to select the grid points right upstream of the main orographic barriers of the regions. Figure 3.1 shows the location of the grid points. The locations differ between the two data sets because they have different horizontal resolutions. As mentioned in the data chapter, the ERA-Interim and 20CR feature a 1° by 1° and 2° by 2° grid respectively. Hereafter, the regions are grouped in northern (Prealps, Eastern Switzerland, Jura) and southern (Ticino, Valais/Alps, Southern Switzerland) Alpine regions.

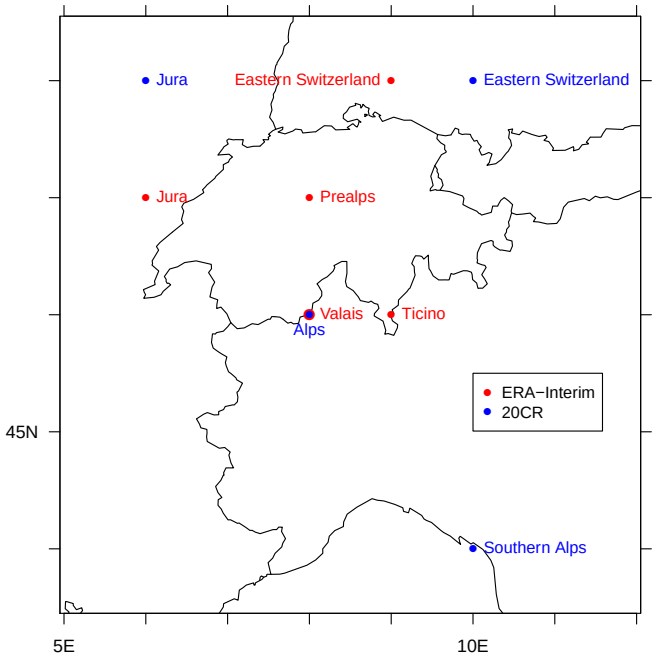

Figure 3.1: Location of the grid points of predefined regions for the ERA-Interim (red) and 20CR (blue) data set respectively.

Chapter 4

Results

The results chapter is seperated in two parts. First, the results of the climtological analyses are presented. The second part shows the main findings resulting from the analyses of the temporal variability of IVT, TPW and steering wind.

4.1 Climatological characteristics

This first part begins with the illustration of the IVT direction and intensity. Second, the yearly cycles of IVT, TPW and steering wind are presented. In the last section, the vertical profiles of moisture flux, specific humditiy and wind speed are shown.

4.1.1 IVT direction and intensity

4.1.1.1 Scatter plots

Northern Alpine regions

Daily mean IVT amplitudes strongly depend on the direction of the flow (Figure 4.1). The patterns are similar in Eastern Switzerland (Figure 4.1a) and Jura (Figure 4.1b). The most intense IVTs come from the South-West and West with maximal intensities of about 600 to 700 $\mathrm{kg\,m^{-1}s^{-1}}$ (Figures 4.1a/b and 4.3a). The maximal intensities of IVTs are much lower from all other directions. A second peak is featured by IVTs coming from the north-easterly direction. These IVTs have intensities above 200 $\mathrm{kg\,m^{-1}s^{-1}}$. However, most of the IVTs have intensities below 200 $\mathrm{kg\,m^{-1}s^{-1}}$. The percentage of intensities below 200 $\mathrm{kg\,m^{-1}s^{-1}}$ is larger than 80% in all three northern Alpine regions (Table 4.1).

Very intense IVTs are more frequent in autumn and summer than in winter and spring. Thus, three-quarter of all IVTs above 400 kg m^{-1}s^{-1} occur in summer and autumn (Table 4.1). IVTs above 400 kg m^{-1}s^{-1} in winter and spring are rare, with percentages of about 15% and 5% in Eastern Swizterland and Jura. The IVTs above 400 kg m^{-1}s^{-1} amount to only 1.6% and 1.8% of all IVTs in Eastern Switzerland and Jura respectively. This percentage is even lower in the Prealps (0.13%). Furthermore, the most intense IVTs coming from the North-East occur almost exclusively in summer.

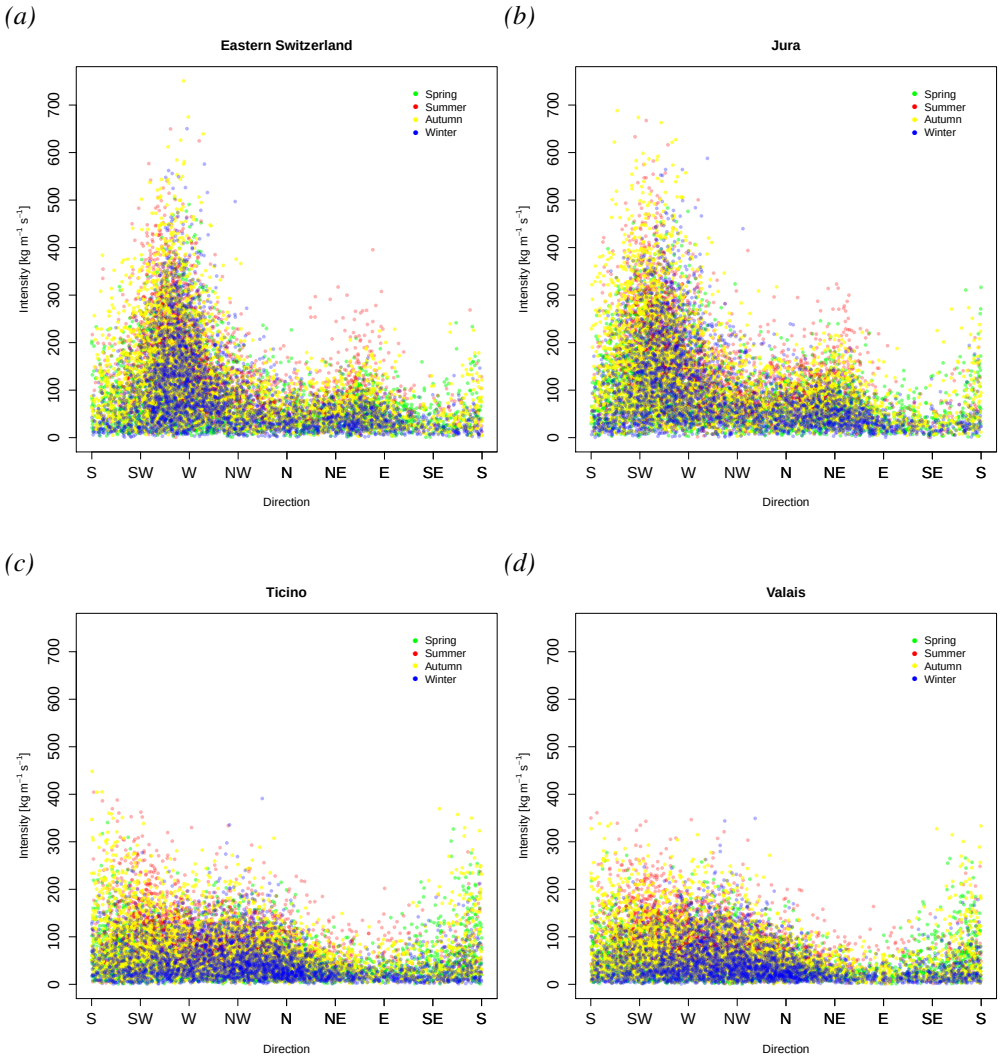

Figure 4.1: Daily mean IVTs of Eastern Switzerland (a), Jura (b), Ticino (c) and Valais (d). The abscissa represents the IVT direction and the oridnate the IVT intensity [kg m^{-1}s^{-1}]. All days of the ERA-Interim time period (1979-2011) are shown with green, red, yellow and blue dots for the days in spring, summer, autumn and winter.

Southern Alpine regions

The maximal intensities are much lower in Ticino (Figure 4.1c) and Valais (Figure 4.1d) compared to the northern Alpine regions. The most intense IVTs have values of about 300 to 400 $\mathrm{kg\,m^{-1}s^{-1}}$ and the perecentage of IVTs below 200 $\mathrm{kg\,m^{-1}s^{-1}}$ is about 97% in both regions (Table 4.1). The most intense IVTs occur in southerly, sout-westerly or westerly fluxes (Figures 4.1c/d and 4.3b).

Regarding the seasonality, the pattern is similar to the northern Alpine pattern. The most intense IVTs occur in autumn and summer. The percentage of IVTs above 200 $\mathrm{kg\,m^{-1}s^{-1}}$ occuring in these seasons represents about 80% of all IVTs above 200 $\mathrm{kg\,m^{-1}s^{-1}}$ (Table 4.1). Thus, IVTs above 200 $\mathrm{kg\,m^{-1}s^{-1}}$ occur rarely in winter (Ticino: 6.9%, Valais: 8.4%) and spring (Ticino: 12.5%, Valais: 8.4%).

	Prealps [%]	**Eastern Switzerland** [%]	**Jura** [%]	**Ticino** [%]	**Valais** [%]
IVTs >200 $\mathbf{kg\,m^{-1}s^{-1}}$	7.6	17.4	18.9	3.0	2.3
Spring	12.7	13.9	15.8	12.5	8.4
Summer	39.3	38.0	35.6	38.2	40.9
Autumn	32.2	29.4	30.0	42.4	42.3
Winter	15.8	18.7	18.7	6.9	8.4
IVTs >400 $\mathbf{kg\,m^{-1}s^{-1}}$	0.13	1.55	1.78	0.03	0
Spring	0	7.0	5.6	0	0
Summer	37.5	34.2	32.7	25.0	0
Autumn	50.0	42.2	46.7	75.0	0
Winter	12.5	16.6	15.0	0	0

Table 4.1: Percentage of daily mean IVTs above 200 (upper rows) and 400 $kg\,m^{-1}s^{-1}$ (lower rows) for each region. In addition, the seasonal percentages are presented for IVTs above the two thresholds. Daily mean IVTs of the ERA-Interim time period (1979-2011) are included.

4.1.1.2 Frequency of IVT direction and intensity

Figure 4.2 shows the distributions of the relative frequency of IVT direction (Figures 4.2a/b) and intensity (Figures 4.2c/d). The relative frequency of IVT direction is shown for each direction covering 45° respectively and the relative frequency of IVT intensity

is shown for each class of 20 kg m^{-1}s^{-1}. Figure 4.3 compelements Figure 4.2 by representing wind rose plots of IVT which show the quartiles and the 95% quantile and their percentage for each 45° sector. The plots are shown for Jura and Ticino, which represent the northern and southern Alpine regions respectively.

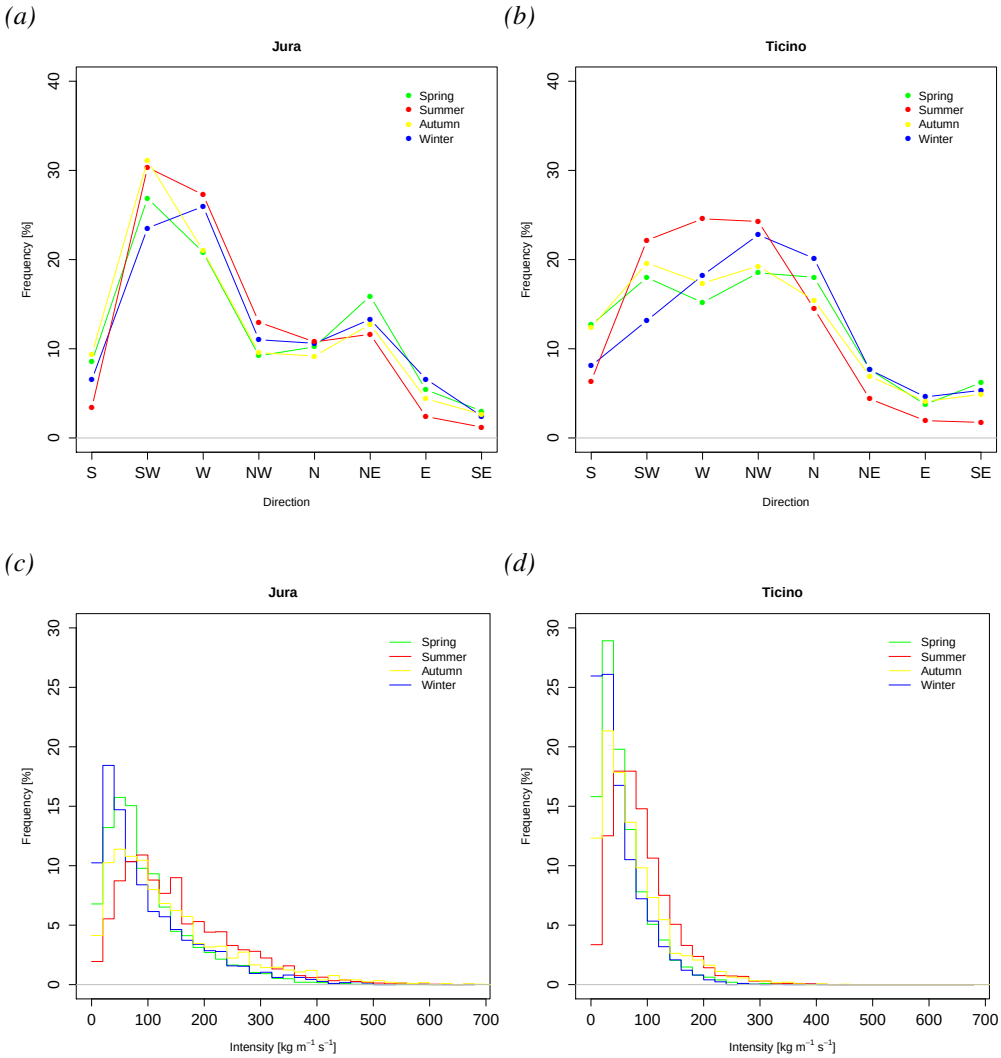

Figure 4.2: (a) and (b): relative frequency of IVT direction for each 45° sector (e.g. S = 157.5°-202.5°). (c) and (d): relative frequency of IVT intensity for each class of 20 kg m^{-1}s^{-1}. Daily mean IVTs of the ERA-Interim time period (1979-2011) are included. The colors indicate the different seasons (green = spring, red = summer, yellow = autumn, blue = winter). The plots are shown for Jura ((a) and (c)) and Ticino ((b) and (d)).

Northern Alpine regions

In Jura, the IVTs come most frequently from the South-West in spring, summer and autumn and from the West in winter (Figure 4.2a). The IVTs originate from these two directions in about 50% of the time (Figure 4.3a). In the Prealps and Eastern Switzerland (Appendix Figures A.2a/c), westerly IVTs are the most frequent in all seasons. In Jura, the frequency of south-easterly IVTs is below 5% in all seasons (Figures 4.2a and 4.3a). Easterly and southerly IVTs are also very rare but have a bigger seasonal variability. IVTs coming from the North-East are the third most frequent IVT direction for all seasons except for summer (Figure 4.2a). The pattern is sligthly different for the Prealps and Eastern Switzerland, where the north-westerly IVTs are the third most frequent (Appendix Figures A.2a/c).

Weak IVTs are more frequent than intense IVTs (Figure 4.2c). In all northern Alpine regions, more than 80% of the IVTs are below 200 $\mathrm{kg\,m^{-1}s^{-1}}$ (Table 4.1). The difference between the seasons is about 10% for some classes (Figure 4.2c). The percentage of IVTs below 200 $\mathrm{kg\,m^{-1}s^{-1}}$ varies with the season. In Jura, the percentages are 73%, 77%, 86% and 88% in summer, autumn, winter and spring respectively (Table 4.1). The percentage of summer IVTs above 150 $\mathrm{kg\,m^{-1}s^{-1}}$ is higher compared to the other seasons except for some classes in autumn. This pattern is even more distinct for the Prealps and Eastern Switzerland (Appendix Figures A.2b/d).

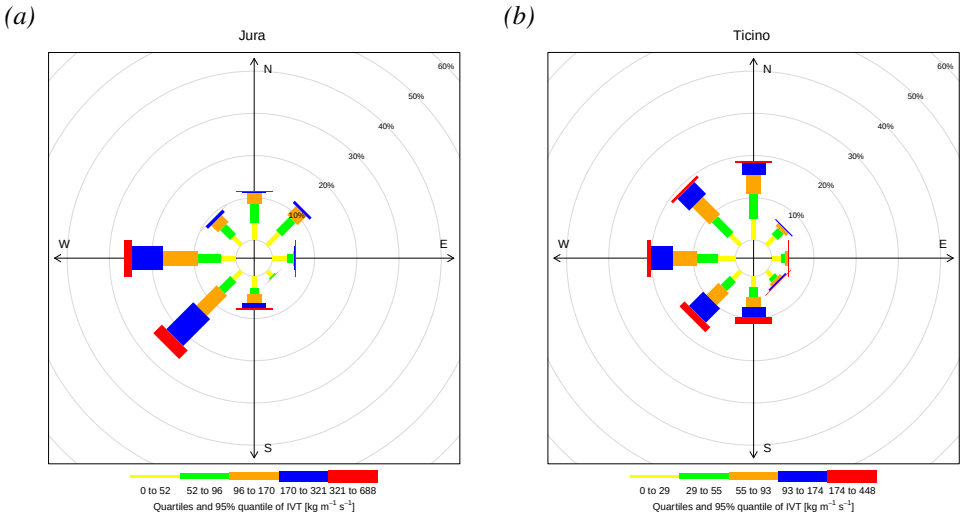

Figure 4.3: Wind rose plots representing the relative frequency of IVT direction for each 45° sector (e.g. S = 157.5°-202.5°) for Jura(a) and Ticino (b). Daily mean IVTs of the ERA-Interim time period (1979-2011) are included. The colors indicate different quantile limits (yellow = 0-25%, green = 25-50%, orange = 50-75%, blue = 75-95%, red = 95-100%) and their percentage for each 45° sector.

Southern Alpine regions

The seasonal variability of the frequency of IVT direction is more pronounced in the southern Alpine regions compared to the northern Alpine regions (Figure 4.2b). South-westerly IVTs are very frequent (around 22%) in summer and less frequent (around 13%) in winter. In summer, moisture arrives preferentially from the South-West, West and North-West (Figure 4.3b). North-westerly and northerly IVTs are up to 10% more frequent in the southern Alpine regions compared to the northern Alpine regions. Southerly IVTs are also more frequent by about 5%. North-easterly IVTs are less frequent (up to 10%) in the southern Alpine regions compared to the northern Alpine regions. IVTs coming from the West or South-West are 5 to 10% less frequent compared to the northern Alpine regions depending on which northern Alpine region is compared to the southern Alpine regions.

Regarding the frequency of the IVT intensity (Figure 4.2d), we see that there is a large seasonal variability of the frequency of the weakest IVTs. In Ticino, the percentage of IVTs below 50 $\mathrm{kg\,m^{-1}s^{-1}}$ varies from around 24% in summer to 61% in winter. All IVTs exceeding 60 $\mathrm{kg\,m^{-1}s^{-1}}$ occur most frequently in summer (Figure 4.2d).

4.1.2 Yearly cycles

4.1.2.1 IVT

The yearly cycle of the IVT (Figure 4.4) shows that the mean intensity of IVT is strongest between June and October. This pattern is similar for all northern and southern Alpine regions. The month with the strongest mean intensity in all regions is July. The range is much wider in the northern Alpine regions than in the southern Alpine regions. The upper whiskers of summer months range to higher values compared to winter months. However, days with very high IVTs can occur throughout the year. If we compare the median of January and July, we see that the medians are in each case outside of the interquartile box of the other month but still within the whisker limits.

4.1.2.2 TPW

The mean intensity of the TPW (Figure 4.5) peaks in the months of July and August. The yearly cycle of TPW shows almost the same pattern in all regions following the mean temperature. The range is shifted to lower values in southern Alpine regions compared to northern Alpine regions. The interquartile ranges reach higher values in summer months compared to winter months. Furthermore, the mean intensity of TPW more than doubles in summer months compared to winter months. There are only few outliers in the yearly cycle of TPW compared to the yearly cycle of IVT. If we compare

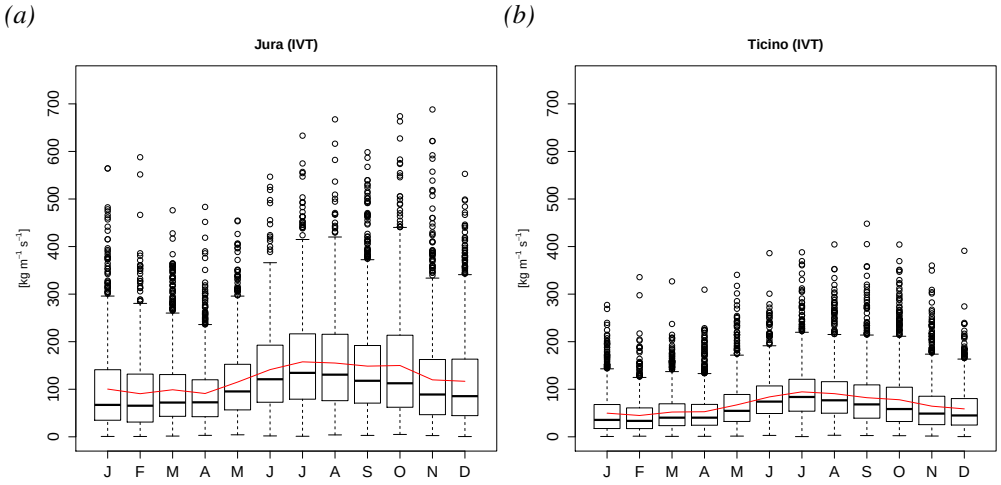

Figure 4.4: Yearly cycle of IVT [kg m^{-1}s^{-1}] shown as boxplots for Jura (a) and Ticino (b). Daily mean IVTs of the ERA-Interim time period (1979-2011) are included. The red line indicates the mean.

the median of January and July similar as we did for IVT, we see that the medians are even outside of the whisker limits of the other month. This shows that the yearly cycle is more distinct for TPW than IVT.

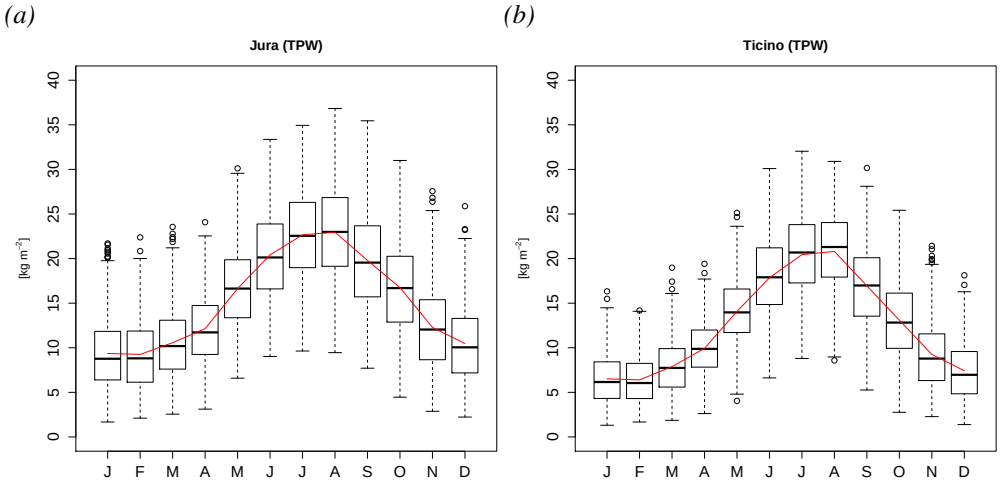

Figure 4.5: Yearly cycle of TPW [kg m^{-2}] shown as boxplots for Jura (a) and Ticino (b). Daily mean values of TPW of the ERA-Interim time period (1979-2011) are included. The red line indicates the mean.

4.1.2.3 Steering wind

The mean intenisity of the steering wind (Figure 4.6) has yearly cycle wihich exhibits an amplitude of about 3 $\mathrm{m\,s^{-1}}$. The yearly cycle of the steering wind is the opposite of the yearly cycle of IVT and TPW, with highest mean intensity in winter and lowest in summer. The upper whiskers of the winter months range also to higher values compared to the summer months. The pattern is similar in northern and southern Alpine regions. However, the intensities are slightly lower in the southern Alpine regions. There are also many outliers throughout the year, as for the yearly cycle of IVT. If the median of January and July are compared, we see that the medians are still within the interquartile box of the other month. This shows that the yearly cycle is not as much distinct for steering wind as for IVT or TPW.

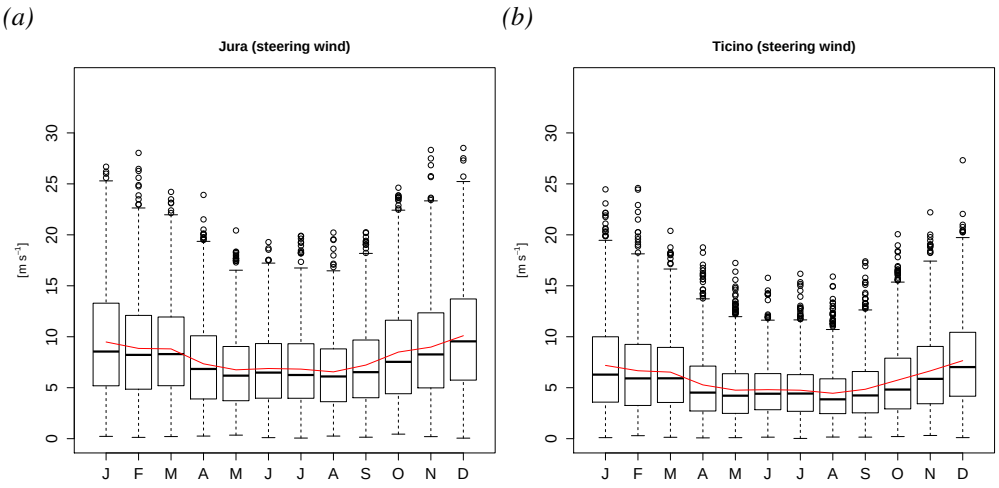

Figure 4.6: Yearly cycle of steeering wind [$m\,s^{-1}$] shown as boxplots for Jura (a) and Ticino (b). Daily mean values of steering wind of the ERA-Interim time period (1979-2011) are included. The red line indicates the mean.

4.1.3 Vertical profiles

4.1.3.1 Moisture flux

Northern Alpine regions

The vertical profile of the moisture flux in Jura (Figure 4.7a) shows that the most intense mean moisture flux occurs in summer. The difference with the mean moisture flux in autumn is minor but this difference is more distinct for the other northern Alpine regions (Prealps, Eastern Switzerland; Appendix Figures A.4a/b). The mean moisture

flux in winter is slightly lower than in spring near the surface (lowest 20 hPa), but gets stronger above this near-surface layer. The mean moisture fluxes in winter and spring are nearly equal above 700 hPa. The strongest intensity of the mean moisture flux occurs almost at the same level ($\sim$ 850 hPa) for all seasons and is halved at about 650 hPa. This is similar in Eastern Switzerland but the level of strongest intensity of the mean moisture flux lies higher ($\sim$ 800 hPa) in the Prealps (Appendix Figures A.4a/b). This strongest intensity varies from 35 to 45 g m^{-2}s^{-1} between the different seasons (Figure 4.7a). This range is shifted to lower values in the Prealps where it varies from around 20 to 30 g m^{-2}s^{-1} (Appendix Figure A.4b). Furthermore, the moisture fluxes above 200 hPa are not relevant anymore.

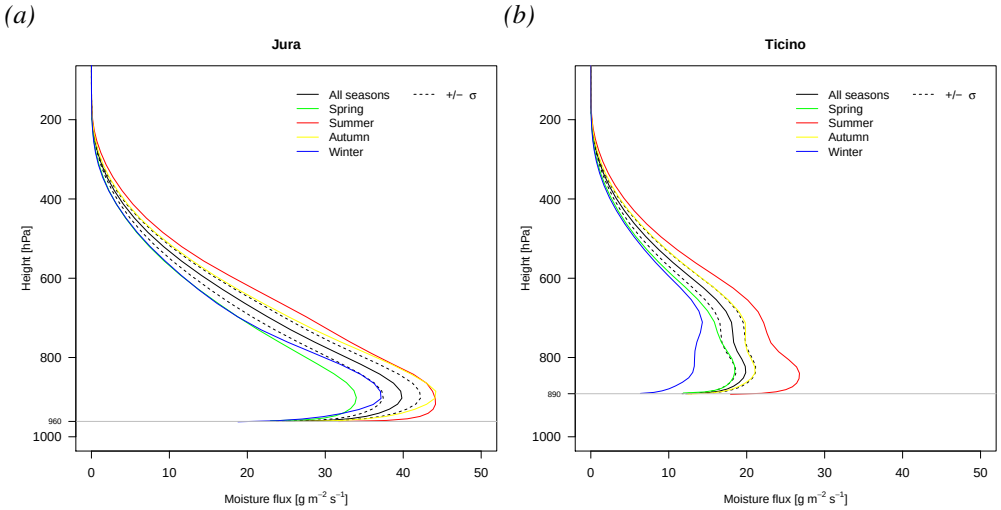

Figure 4.7: Mean vertical profile of the moisture flux [g m^{-2}s^{-1}] at 12 UTC including all days of the ERA-Interim time period (1979-2011). The colors of the lines present the seasons with green, red, yellow and blue indicating the mean intensity in spring, summer, autmn and winter. The black line shows the mean over all seasons and the dashed black lines limit the range from plus to minus one standard deviation from the yearly means. The vertical profile is shown for Jura (a) and Ticino (b).

Southern Alpine regions

Figure 4.7b shows the vertical profile of the moisture flux in Ticino. In contrast to Jura, the mean moisture flux in winter is at all levels lower than in spring. Another difference is that the most intense mean moisture flux is halved at about 550 hPa, which is about 100 hPa lower compared to the northern Alpine regions. However, it is not possible to define one specific level at which the mean moisture fluxes of the different seasons are most intense. While the level of the strongest intensity lies at 700 hPa in winter it is situated at 800 hPa during the other seasons. This strongest intensity varies between about 15 to 25 g m^{-2}s^{-1} between the different seasons.

4.1.3.2 Specific humidity

Northern Alpine regions

The vertical profile of the seasonal mean of specific humidity in Jura is presented in Figure 4.8a. A distinct seasonal cycle is visible, especially near the surface where it ranges from 4 g kg^{-1} in winter to about 8.5 g kg^{-1} in summer. The surface describes also the level at which the seasonal mean of specific humidities are the highest. The specific humidity decreases significantly with height. Therefore, the seasonal means of specific humidity are halved at about 750 hPa and reach values of only 1 g kg^{-1} at the 500 hPa level. The patterns are similar in the Prealps and Eastern Switzerland except that the range of the near-surface seasonal mean of specific humidity is shifted to lower values ($\sim$ 3.5-8 g kg^{-1}) in the Prealps (Appendix Figures A.4d/e).

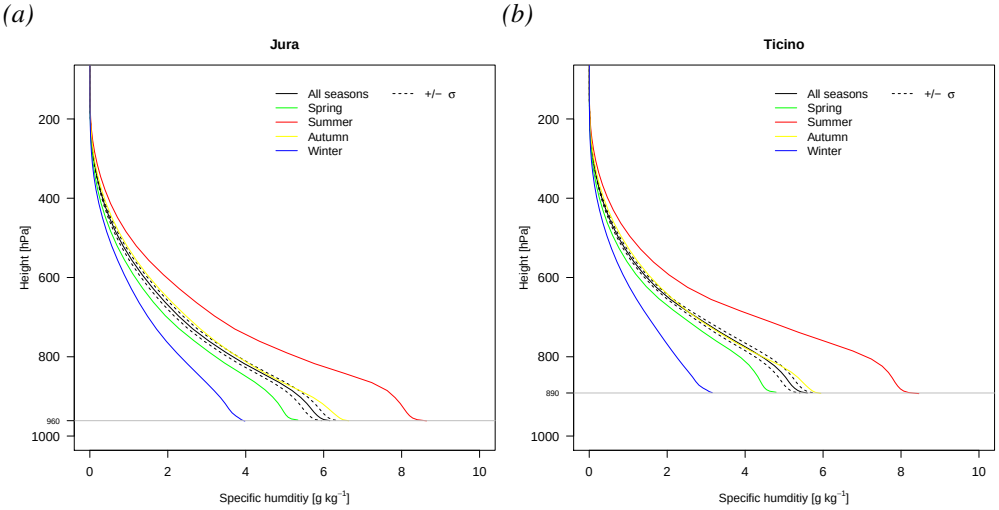

Figure 4.8: Mean vertical profile of the specific humidity [g kg^{-1}] at 12 UTC including all days of the ERA-Interim time period (1979-2011). The colors of the lines present the seasons with green, red, yellow and blue indicating the mean intensity in spring, summer, autmn and winter. The black line shows the mean over all seasons and the dashed black lines limit the range from plus to minus one standard deviation from the yearly means. The vertical profile is shown for Jura (a) and Ticino (b).

Southern Alpine regions

The vertical profile of the seasonal mean of specific humidity in Ticino (Figure 4.8b) features the same seasonal cycle as northern Alpine regions. Furthermore, the specific humidity decreases also significantly with height, resulting that the mean specific humidity is halved at about 700 hPa. In Ticino, values of the near-surface seasonal mean of specific humidity range from 3.5 in winter to about 8.5 g kg^{-1} in summer.

This range is slightly wider compared to the northern Alpine regions. However, it is different in Valais where a shift to lower values is observed and the range is slightly narrower ($\sim$ 3-7.5 g kg^{-1}; Appendix Figure A.4f).

4.1.3.3 Wind speed

Northern Alpine regions

The vertical profile of the seasonal mean of wind speed in Jura (Figure 4.9a) shows increasing wind speed from the surface up to 300 hPa where it peaks at about 20 to 25 m s^{-1}, depending on the season. However, the wind speed decreases rapidly above 300 hPa. The differences between the seasonal mean of wind speed vary between 1 to 5 m s^{-1} over the vertical profile. The mean wind speed is strongest in winter and lowest in summer except for a short section above 300 hPa at which the mean wind speed in spring is lowest. The wind speed increases more rapidly with height from the surface up to 800 hPa in winter ($\sim$ 4.7 m s^{-1} / 100 hPa) than during the other seasons (2-3.5 m s^{-1} / 100 hPa). The overall pattern of the vertical profile is similar in Eastern Switzerland and in the Prealps except that the wind speed is lower near the surface in the Prealps compared to the other two regions (Appendix Figures A.4g/h).

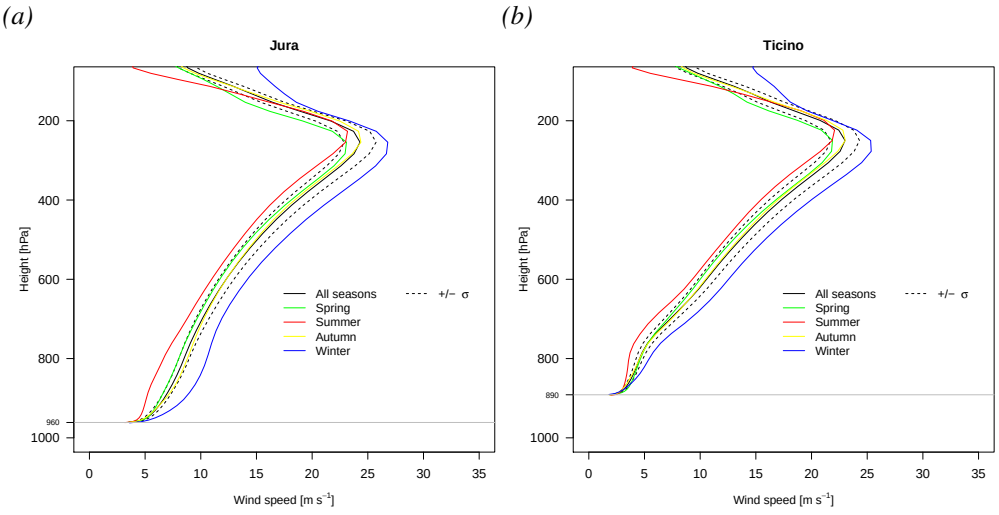

Figure 4.9: Mean vertical profile of the wind speed [m s^{-1}] at 12 UTC including all days of the ERA-Interim time period (1979-2011). The colors of the lines present the seasons with green, red, yellow and blue indicating the mean intensity in spring, summer, autmn and winter. The black line shows the mean over all seasons and the dashed black lines limit the range from plus to minus one standard deviation from the yearly means. The vertical profile is shown for Jura (a) and Ticino (b).

Southern Alpine regions

The vertical profile of the seasonal mean of wind speed in Ticino (Figure 4.9b) shows a comparable pattern to the vertical profile of Jura. However, two features are different. First, the wind speed is lower near the surface and second, there is a kink in the vertical profile at about 750 hPa. At this kink there is a transition from a weaker ($\sim 2.5\,\mathrm{m\,s^{-1}}$ / 100 hPa) to a stronger ($\sim 3.6\,\mathrm{m\,s^{-1}}$ / 100 hPa) gradient in increasing wind speed with height. The kink is even more distinct in Valais (Appendix Figure A.4i). Apart from that, the vertical profiles of the two southern Alpine regions are almost identical.

4.2 Temporal variability

In this section, the results of the analyses of the temporal variability of IVT, TPW and steering wind are shown. First, the analyses of the interannual variability are presented followed by the wavelet analyses. The trends for the ERA-Interim and 20CR time periods conclude this section.

4.2.1 Interannual variability

The plots in Figure 4.10 show the yearly mean of IVT, TPW and steering wind as relative deviation from the long-term mean of the ERA-Interim time period between 1979 and 2011 for Jura and Ticino. The plots in Figure 4.11 show the same as Figure 4.10 for IVT but include additionally the data of 20CR.

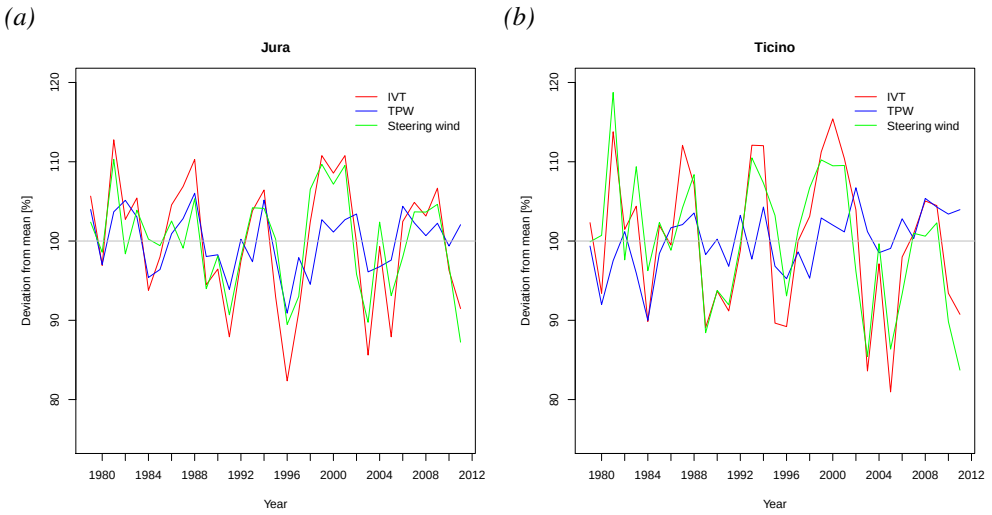

Figure 4.10: Yearly mean of IVT, TPW and steering wind as relative deviation from the long-term mean of the ERA-Interim time period (1979-2011) in Jura (a) and Ticino (b). The red, blue and green line show the yearly mean of IVT, TPW and steering wind.

IVT

The plots in Figure 4.10 show that the yearly mean of IVT varies around plus and minus 15% around the long-term mean. The variations are slightly higher in Ticino compared to Jura. The time series seem to feature a cycle of around 6 years. The other regions show a similar pattern with similar amplitudes (Appendix Figures A.5a-c).

The plots in Figure 4.11 show that the IVT exhibit a similar pattern of interannual variability in the end of the 20th century for 20CR and ERA-Interim data. The amplitudes in Jura and Alps are mostly slightly higher for ERA-Interim data than for 20CR data.

TPW

The interannual variability of TPW has a samller amplitude (<10%) compared to the interannual variability of IVT. While the time series of Jura is highly correlated with the IVT time series, the time series of Ticino does not show statistically significant correlation (Table 4.2). The remaining regions exhibit similar patterns as Jura, including a similar 6 year cycle (Appendix Figures A.5a-c).

Steering wind

The steering wind follows almost the same pattern of interannual variability as the IVT. The amplitudes are only slightly lower than those of IVT. In Ticino and also in Valais (Appendix Figure A.5c), the variation of the yearly mean of steering wind in 1981 exceeds the variation of the yearly mean the IVT.

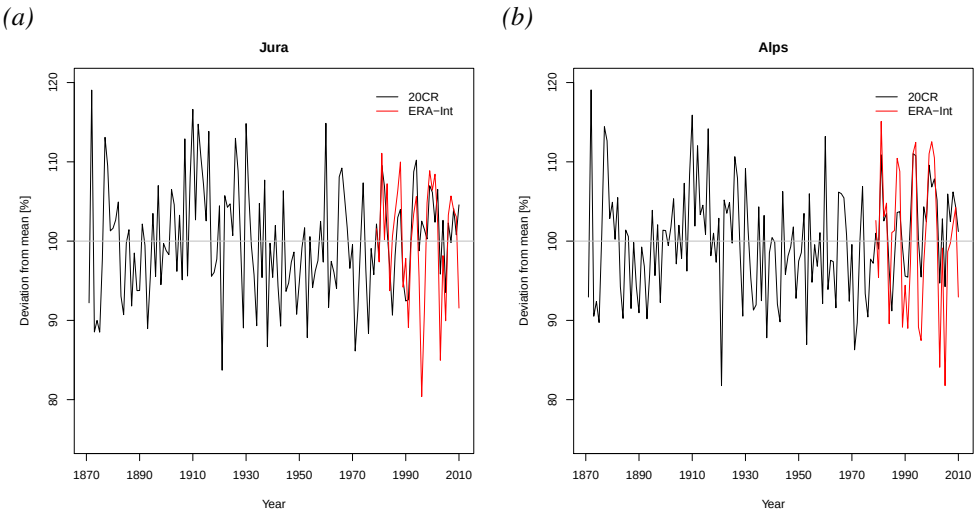

Figure 4.11: Yearly mean of IVT as relative deviation from the long-term mean of the 20CR time period (1871-2010; black) and from the long-term mean of the ERA-Interim time period (1979-2011; red) in Jura (a) and Alps (b). The grid point of Jura for the ERA-Interim data is adjusted to the grid point of Jura for the 20CR data (Figure 3.1).

4.2.1.1 Linear regression models

Consequently, the variation of the yearly mean of TPW, steering wind or wind on a certain pressure level is used to explain the interannual variability of the IVT. Therefore, an univariate linear regression model with one of these variables is fitted for IVT. Table 4.2 shows the explained variance R^2. It provides a measure of how much of the total variation of the IVT is explained by the linear regression model.

The TPW explains between 42 and 56% of the yearly variation of IVT in northern Alpine regions. In contrast, it explains only 11% and 25% of the total variation of IVT in Ticino and Valais. Furthermore, the hypothesis can not be rejected that the linear regression model for Ticino is not statistically significant at the 5% significance level. The steering wind is a better predictor for IVT compared to TPW, because it explains between 73 and 87% of the total variation of IVT. It can be distinguished between northern and southern Alpine regions. The R^2 is about (Jura) or clearly above (Prealps, Eastern Switzerland) 80% in northern Alpine regions, whereas the R^2 is clearly below 80% in southern Alpine regions.

The same analysis is carried out for the wind on a certain pressure level, in order to compare its R^2 with the R^2 of steering wind. Therefore, the linear regression model was calculated in steps of 50 hPa. Table 4.2 shows only the pressure levels where the R^2 is maximal for a region. The wind at 750 hPa explains about 80% and 88% of the total variation of IVT in Jura and Eastern Switzerland. For Eastern Switzerland, this R^2 is even slightly higher than the R^2 of steering wind. R^2 is maximal for the wind at 700 hPa in the Prealps (83%). The maximal R^2 occurs for the wind at 650 hPa in the southern Alpine regions (Ticino: 81%, Valais: 79%).

R^2	**TPW**	**Steering wind**	**Wind @ 750 hPa**	**Wind @ 700 hPa**	**Wind @ 650 hPa**
Prealps	0.419	0.830	0.793	0.831	0.825
Eastern Switzerland	0.445	0.868	0.883	0.869	0.842
Jura	0.559	0.798	0.797	0.789	0.763
Ticino	(0.113)	0.732	0.676	0.773	0.808
Valais	0.247	0.769	0.592	0.722	0.791

Table 4.2: Explained variance R^2 of different linear regression models for IVT in the Prealps, Eastern Switzerland, Jura, Ticino and Valais. Value in brackets is not statistically significant at the 5% significance level.

4.2.2 Wavelet analyses

The CWT power spectra are depicted for the different variables (IVT, TPW, steering wind) and regions. First, the results are shown for ERA-Interim data and secondly for 20CR data.

4.2.2.1 ERA-Interim

IVT

The plots in Figure 4.12 display the CWT power spectrum of the standardised yearly mean of IVT in Jura and Ticino. The time series show statistically significant wavelet power at periods between about 5 and 8 years. The time series of the other regions (Prealps, Eastern Switzerland, Valais; Appendix Figures A.6a-c) feature statistically significant wavelet power in the same oscillation band as the time series of Jura and Ticino. However, the oscillation bands are partly outside of the COI due to the limited length of the ERA-Interim time period.

Regarding the CWT power spectra of the standardised seasonal mean of IVT in Jura (Figure 4.13), we find statistically significant oscillation bands during all seasons, which range between 5 and 8 years. The oscillation bands are less distinct during spring and summer compared to autumn and winter. During spring and summer, there are also statistically significant wavelet power at higher freqeuencies, namely at peri-

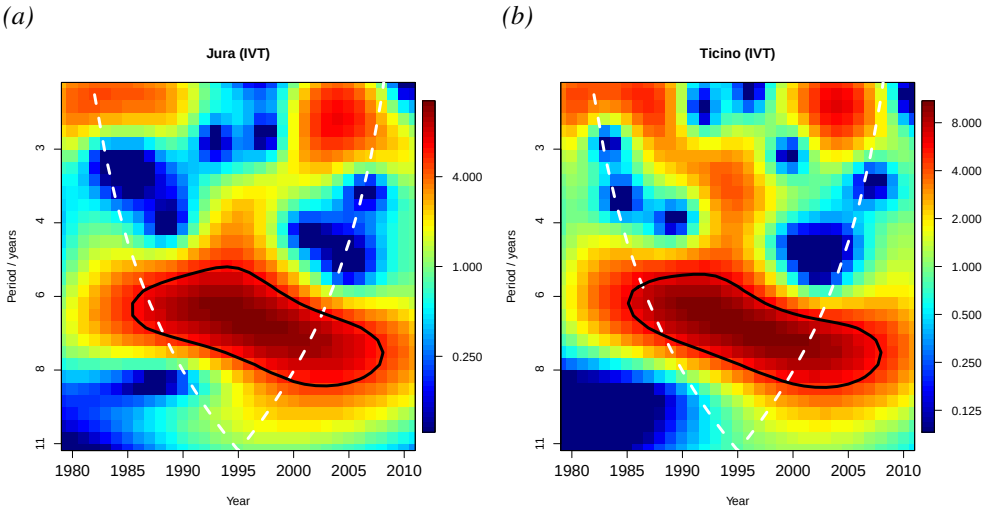

Figure 4.12: CWT power spectra of the standardised yearly mean of IVT in Jura (a) and Ticino (b) for the ERA-Interim time period (1979-2011). The abscissa indicates the time and the ordinate features the period in years. The black contour lines show the 5% significance level. The dashed white line denotes the COI where edge effects become important.

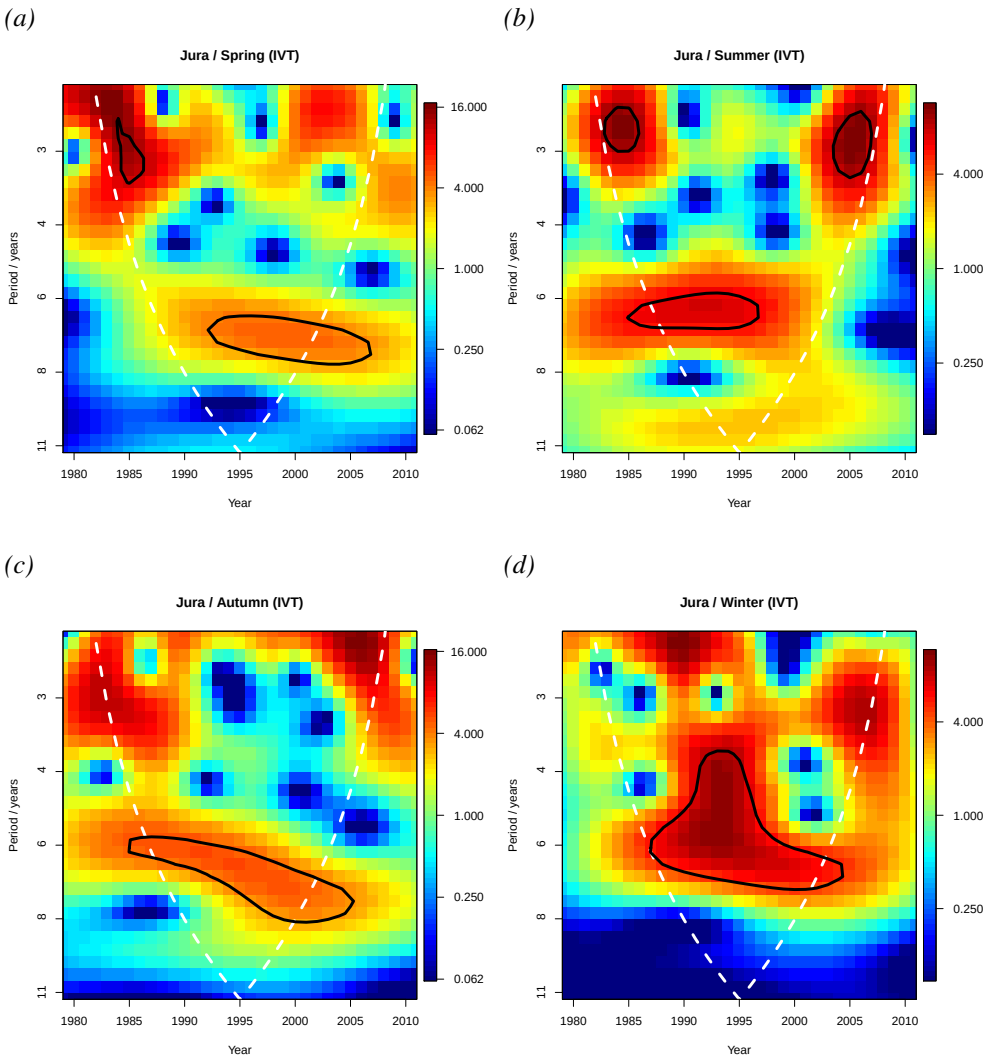

Figure 4.13: CWT power spectra of the standardised seasonal mean of IVT in Jura for the ERA-Interim time period (1979-2011). The abscissa indicates the time and the ordinate features the period in years. The black contour lines show the 5% significance level. The dashed white line denotes the COI where edge effects become important.

ods of about 3 years. The statistically significant oscillation band in winter reveals a wide range in the 1990s. The remaining regions feature almost the same characteristics of the CWT power spectra of the standardised seasonal mean of IVT as Jura but there are also some differences. The statistically significant oscillation band in autumn is almost not distinguishable in Eastern Switzerland, whereas the oscillation bands between 5 and 8 years in spring and summer are more pronounced in all other regions compared to Jura. Furthermore, the remaining regions feature the same pattern for the winter oscillation band but the southern Alpine regions show additionally statistically significant wavelet power at periods of about 3 years.

TPW

The panels in Figure 4.14 show the CWT power spectrum of the standardised yearly mean of TPW in Jura and Ticino. The plot for Jura reveals statistically significant wavelet power at periods between about 5 and 8 years similar to the results of IVT. However, the time series of Ticino does not feature a statistically significant oscillation band between 5 and 8 years. Nevertheless, all other regions (Prealps, Eastern Switzerland, Valais; Appendix Figures A.6d-f) present the same statistically significant wavelet power as the time series of Jura.

The CWT power spectra of the standardised seasonal mean of TPW are presented in Figure 4.15 for Jura. The time series of seasonal mean of TPW in spring features a distinct statistically significant oscillation band between 6 and 8 years. The time series of the other seasons (summer, winter) show patchy oscillation bands or a slightly pronounced statistically significant oscillation band (autumn). The other regions feature almost the same patterns of the CWT power spectra of the standardised seasonal mean of TPW as Jura. However, the pattern is different in summer for the southern Alpine regions where only hardly visible (Ticino) or no (Valais) statistically significant oscillation bands are observed.

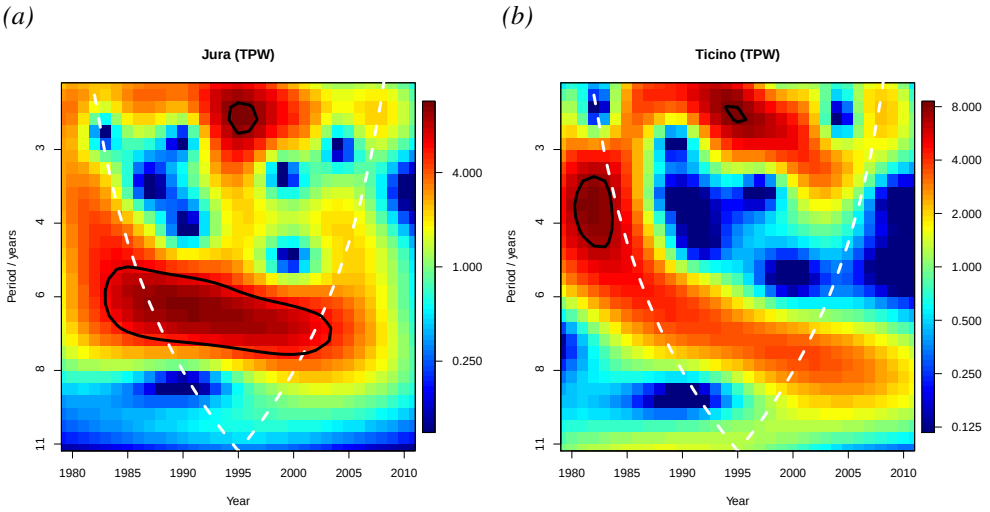

Figure 4.14: CWT power spectra of the standardised yearly mean of TPW in Jura (a) and Ticino (b) for the ERA-Interim time period (1979-2011). The abscissa indicates the time and the ordinate features the period in years. The black contour lines show the 5% significance level. The dashed white line denotes the COI where edge effects become important.

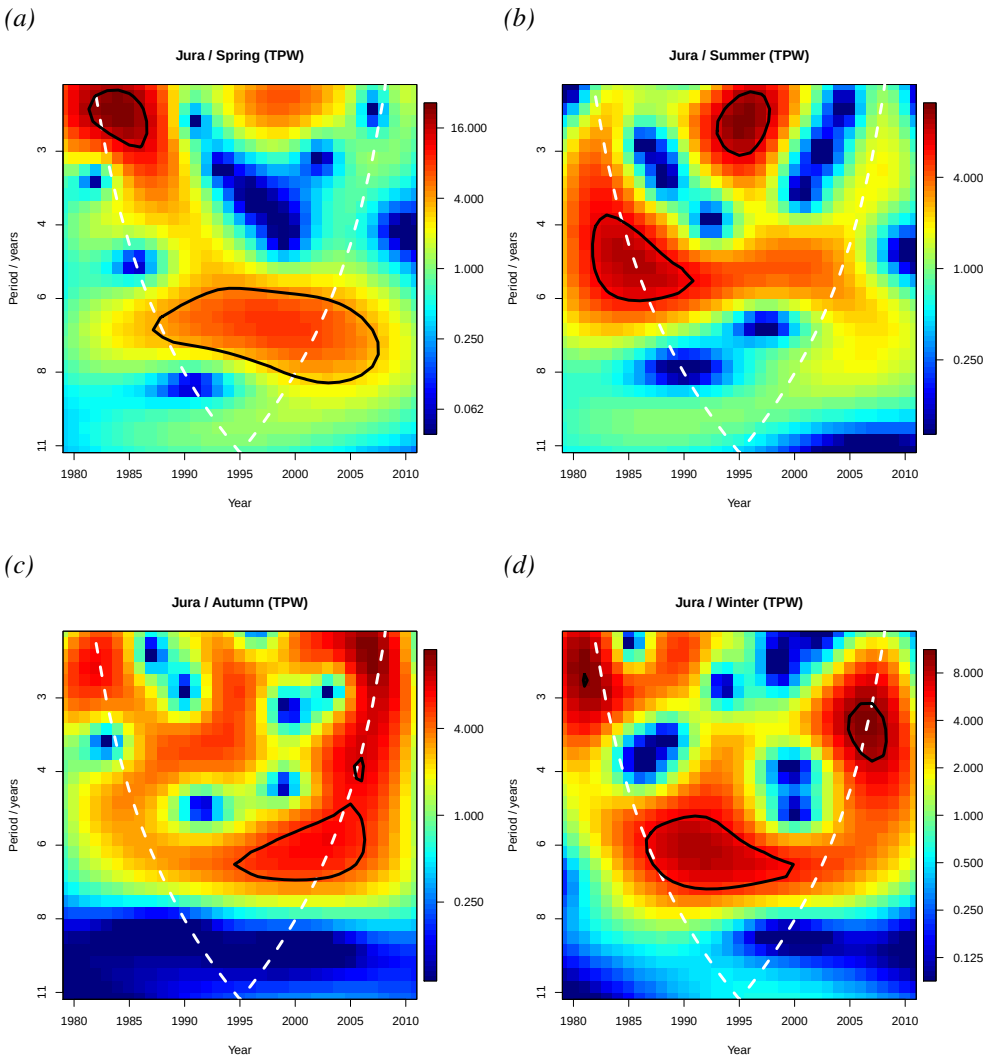

Figure 4.15: CWT power spectra of the standardised seasonal mean of TPW in Jura for the ERA-Interim time period (1979-2011). The abscissa indicates the time and the ordinate features the period in years. The black contour lines show the 5% significance level. The dashed white line denotes the COI where edge effects become important.

Steering wind

The plots in Figure 4.16 show the CWT power spectrum of the standardised yearly mean of steering wind in Jura and Ticino. The time series of Jura and Ticino feature statistically significant wavelet power at periods between 5 and 8 years. The time series of the other regions (Prealps, Eastern Switzerland, Valais; Appendix Figures A.6g-i) show the same features.

The CWT power spectra of the standardised seasonal mean of steering wind are shown in Figure 4.17 for Jura. The winter time series shows a similar pattern of the statisti-

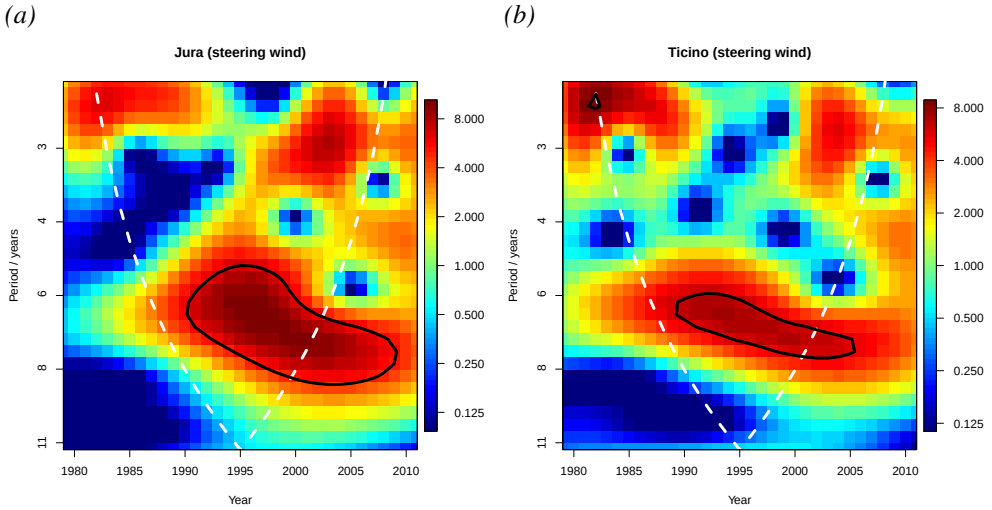

Figure 4.16: CWT power spectra of the standardised yearly mean of steering wind in Jura (a) and Ticino (b) for the ERA-Interim time period (1979-2011). The abscissa indicates the time and the ordinate features the period in years. The black contour lines show the 5% significance level. The dashed white line denotes the COI where edge effects become important.

cally significant oscillation band as the one of the winter IVT (Figure 4.13d). The time series of summer and autumn show patchy oscillation bands, namely at higher ($\sim$ 6-8 years) and lower ($\sim$ 3 years) frequencies. However, the oscillation band at lower frequencies is pronounced during autumn. The time series in spring does not feature any statistically significant oscillation band. The other regions show some differences but also some similarities to the wavelet plots of Jura. The time series in winter present almost the same pattern in all the other regions as Jura. This is also true for the time series in spring. The Prealps and Eastern Switzerland feature a more distinct oscillation band between 6 and 8 years in summer, whereas the southern Alpine regions show a less distinct oscillation band at these frequencies. The southern Alpine regions do not exhibit any statistically significant oscillation band in autumn in contrast to the northern Alpine regions.

4.2.2.2 20CR

IVT

The plots in Figure 4.18 show the CWT power spectrum of the standardised yearly mean of IVT in Jura and the Alps. The time series reveal statistically significant wavelet power at periods between 5 and 8 years from about 1960 to the end of the 20th century, similar to the time series of ERA-Interim (Figure 4.12). However, the time series show also a patchy pattern with statistically significant wavelet power at

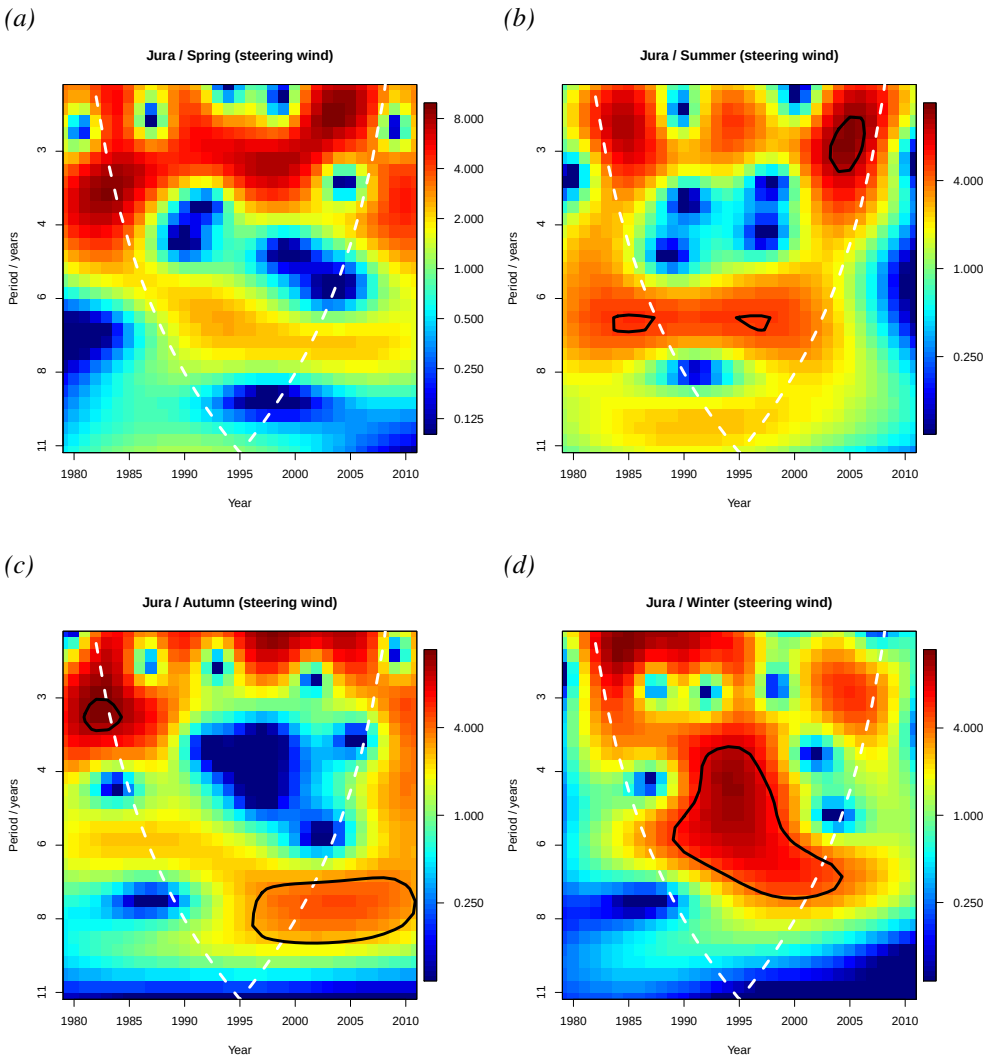

Figure 4.17: CWT power spectra of the standardised seasonal mean of steering wind in Jura for the ERA-Interim time period (1979-2011). The abscissa indicates the time and the ordinate features the period in years. The black contour lines show the 5% significance level. The dashed white line denotes the COI where edge effects become important.

higher and lower frequencies. The time series of the Southern Alps exhibits also a statistically significant wavelet power in the oscillation band between 5 and 8 years in the end of the 20th century (Appendix Figure A.7b). In contrast, Eastern Switzerland does not show a statistically significant wavelet power at those periods (Appendix Figure A.7a). All regions have common statistically significant wavelet power at periods higher than 32 years. This oscillation band is most distinct for the Alps (Figure 4.18b).

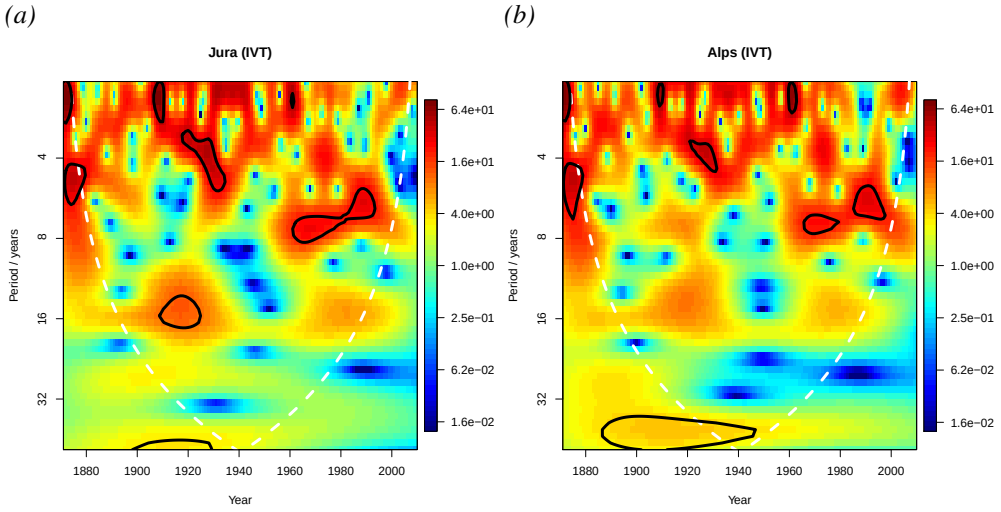

Figure 4.18: CWT power spectra of the standardised yearly mean of IVT in Jura (a) and Alps (b) for the 20CR time period (1871-2010). The abscissa indicates the time and the ordinate features the period in years. The black contour lines show the 5% significance level. The dashed white line denotes the COI where edge effects become important.

TPW

The plots in Figure 4.19 show the CWT power spectrum of the standardised yearly mean of TPW in Jura and the Alps. The time series exhibit statistically significant wavelet power at periods between 5 and 8 years towards the end of the 20th century.

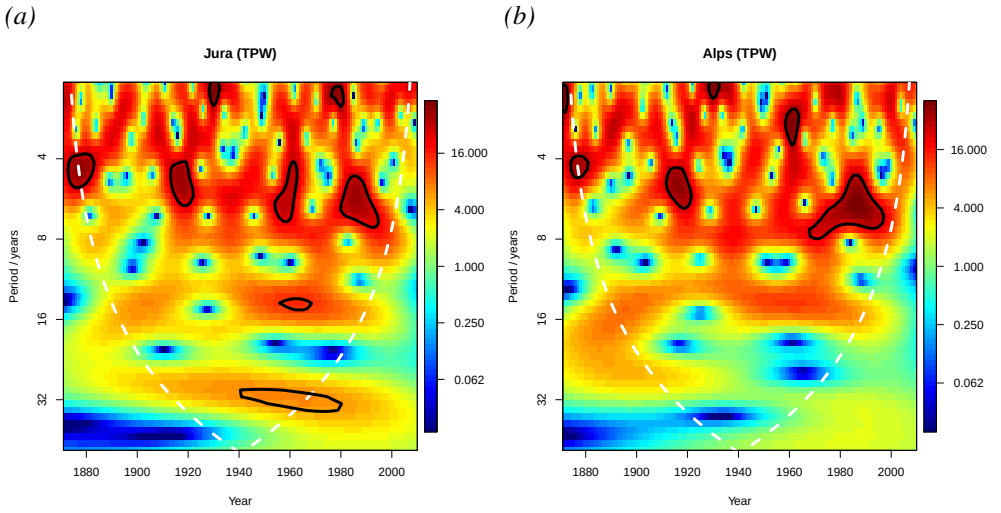

Figure 4.19: CWT power spectra of the standardised yearly mean of TPW in Jura (a) and Alps (b) for the 20CR time period (1871-2010). The abscissa indicates the time and the ordinate features the period in years. The black contour lines show the 5% significance level. The dashed white line denotes the COI where edge effects become important.

This pattern is also visible for the Southern Alps but not for Eastern Switzerland (Appendix Figures A.7c/d), which reproduces the same characetristics as those of the time series of IVT. Jura is the only region which features statistically significant wavelet power at lower frequencies, namely at periods about 32 years.

Steering wind

The plots in Figure 4.20 show the CWT power spectrum of the standardised yearly mean of steering wind in Jura and the Alps. Both times series do not show statistically significant wavelet power at periods between 5 and 8 years towards the end of the 20th century. This contrasts with the previous time series of IVT and TPW. Furthermore, the time series of Eastern Switzerland and Southern Alps do not feature statistically significant wavelet power in this range (Appendix Figures A.7e/f). All regions show a patchy pattern of statistically significant wavelet power but it can be summarized that all time series of the different regions have common statistically significant wavelet power at periods higher than 32 years.

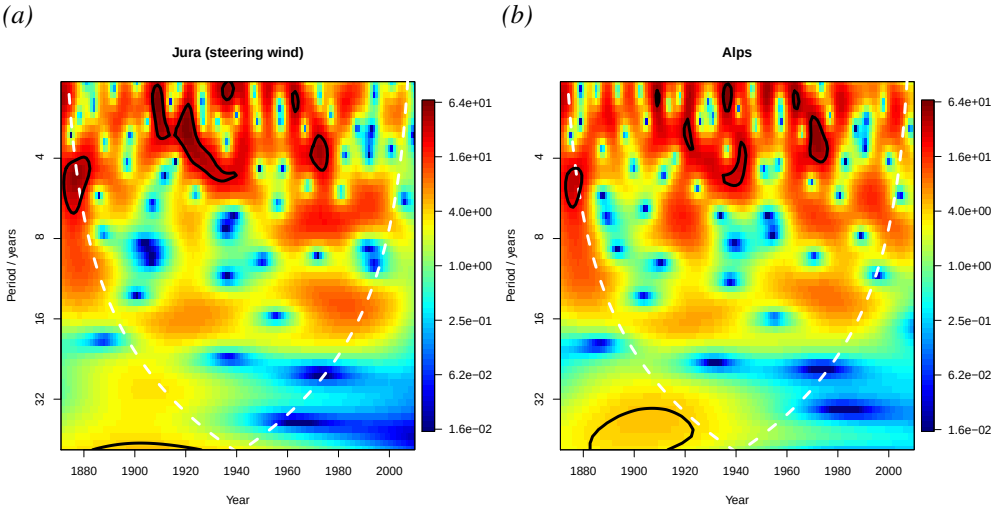

Figure 4.20: CWT power spectra of the standardised yearly mean of steering wind in Jura (a) and Alps (b) for the 20CR time period (1871-2010). The abscissa indicates the time and the ordinate features the period in years. The black contour lines show the 5% significance level. The dashed white line denotes the COI where edge effects become important.

4.2.3 Trend analyses

First, the results are represented for ERA-Interim data and then for 20CR data. The trends are presented for the mean, the 90% quantile and the maximum of IVT, TPW and steering wind.

4.2.3.1 ERA-Interim

Trends of the mean

Table 4.3 shows the trends of the seasonal and yearly mean of IVT, TPW and steering wind. The seasonal mean of IVT features only negative trends in all regions and seasons, except during summer in the Prealps, Jura, Ticino and Valais. The negative trends for autumn and winter are stronger in all regions than for spring. All regions exhibit negative trends of the yearly mean of IVT. However, no trend is statistically significant at the 5% significance level.

The seasonal mean of TPW features negative trends in all regions for autumn and winter, except in Ticino for autumn. Positive trends are detected in all regions for spring and summer. The summer trends are statistically significant in the Prealps, Ticino and Valais. The trend of the yearly mean of TPW is positive in the Prealps, Eastern Switzerland, Ticino and Valais. However, the trend is only statistically significant in Ticino.

The trends for the seasonal mean of steering wind are all negative, except in Jura for summer when the trend is about zero. The negative trends for autumn and winter are stronger in all regions than for spring or summer, except in Jura where the trend is most negative for spring. The yearly mean of steering wind shows a negative trend in all regions. However, no trend of steering wind is statistically significant similarly to the trends of IVT.

Trends of the 90% quantile

Table 4.4 shows the trends of the seasonal and yearly 90% quantile of IVT, TPW and steering wind. The seasonal 90% quantile of IVT features in all regions positive trends for spring (except in Valais) and summer and negative trends for autumn and winter. The trends are statistically significant in the Prealps and Eastern Switzerland for autumn and in Ticino for winter. The trends of the yearly 90% quantile of IVT are all negative but not statistically significant.

The seasonal 90% quantile of TPW features positive trends in all regions for spring and summer. The summer trends are statistically significant in the Prealps, Ticino

Trends of the mean [%/decade]	**Spring**	**Summer**	**Autumn**	**Winter**	**Year**
IVT					
Prealps	-1.1	0.1	-4.4	-4.4	-2.2
Eastern Switzerland	-0.5	-0.4	-4.5	-3.0	-2.1
Jura	-1.6	1.0	-2.9	-2.9	-1.4
Ticino	-0.5	0.7	-3.1	-3.6	-1.4
Valais	-0.6	0.2	-4.0	-4.4	-1.9
TPW					
Prealps	1.3	**1.8**	-0.5	-2.3	0.5
Eastern Switzerland	0.7	1.1	-0.6	-1.5	0.2
Jura	0.8	0.7	-0.7	-2.5	-0.1
Ticino	2.4	**3.3**	0.9	-0.4	**2.0**
Valais	1.9	**2.3**	-0.2	-1.8	1.0
Steering wind					
Prealps	-2.3	-1.6	-2.8	-2.9	-2.4
Eastern Switzerland	-1.2	-1.6	-2.9	-1.8	-1.9
Jura	-2.0	0.0	-1.0	-1.3	-1.0
Ticino	-2.1	-2.3	-3.1	-3.7	-2.9
Valais	-2.1	-1.9	-3.0	-3.5	-2.7

Table 4.3: Trends [%/decade] of the seasonal and yearly mean of IVT (upper rows), TPW (middle rows) and steering wind (lower rows) for each region and each season. The trends are calculated from 1979 to 2011. Bold values are statistically significant trends at the 5% significance level for two-sided tests.

and Valais. For autumn, the trends are also positive in three regions (Prealps, Eastern Switzerland, Ticino) but for winter, the trends are negative in all regions, except in Ticino. The yearly 90% quantile of TPW shows positive trends in all regions which are also statistically significant in the Prealps, Ticino and Valais.

The trends for the seasonal 90% quantile of steering wind are all negative, except in Jura during summer. The negative trends for winter are stronger in all regions than the trends for the other seasons, except in Eastern Switzerland where the trend is most negative for autumn. The trends for winter are also statistically significant in Ticino

Trends of the 90% quantile [%/decade]	**Spring**	**Summer**	**Autumn**	**Winter**	**Year**
IVT					
Prealps	0.9	1.2	**-5.9**	-4.4	-2.4
Eastern Switzerland	0.9	0.1	**-5.9**	-3.8	-2.5
Jura	0.9	1.6	-4.3	-2.2	-0.7
Ticino	0.3	2.8	-0.9	**-6.0**	-1.6
Valais	0.0	1.8	-2.8	-4.9	-2.2
TPW					
Prealps	2.4	**1.6**	0.1	-2.6	**1.8**
Eastern Switzerland	1.5	1.1	0.1	-2.2	1.1
Jura	1.2	1.1	-0.2	-2.8	0.7
Ticino	3.0	**3.4**	1.2	0.2	**2.9**
Valais	2.4	**2.4**	-0.4	-1.6	**2.0**
Steering wind					
Prealps	-1.8	-0.4	-3.2	-4.5	**-2.5**
Eastern Switzerland	-2.1	-1.2	-3.6	-3.1	-2.2
Jura	-0.4	0.9	-0.9	-1.9	-1.6
Ticino	-2.3	-2.6	-2.8	**-5.5**	**-3.5**
Valais	-0.7	-1.6	-3.5	**-5.7**	**-3.0**

Table 4.4: Trends [%/decade] of the seasonal and yearly 90% quantile of IVT (upper rows), TPW (middle rows) and steering wind (lower rows) for each region and each season. The trends are calculated from 1979 to 2011. Bold values are statistically significant trends at the 5% significance level for two-sided tests.

and Valais. All regions show negative trends of the yearly 90% quantile of steering wind and they are statistically significant in three regions (Prealps, Ticino, Valais).

Trends of the maximum

Table 4.5 shows the trends of the seasonal and yearly maximum of IVT, TPW and steering wind. The seasonal maximum of IVT features in all regions positive trends for summer and negative trends for autumn and winter. The trends for spring are positive

Trends of the maximum [%/decade]	**Spring**	**Summer**	**Autumn**	**Winter**	**Year**
IVT					
Prealps	3.6	2.5	**-7.8**	-0.5	-3.0
Eastern Switzerland	1.6	3.3	-5.2	-2.5	-0.4
Jura	2.7	1.7	-6.0	-0.7	-2.8
Ticino	-5.8	1.2	-7.4	-0.7	-3.8
Valais	-2.0	1.2	**-7.0**	-1.7	-3.0
TPW					
Prealps	**4.1**	**1.8**	2.5	-1.3	2.1
Eastern Switzerland	3.9	1.0	2.7	-1.1	1.2
Jura	2.3	0.5	2.5	-2.6	0.8
Ticino	**3.8**	2.1	1.3	0.0	1.9
Valais	**4.1**	**2.6**	1.4	-0.2	2.6
Steering wind					
Prealps	-1.2	1.8	-4.2	-0.8	-0.3
Eastern Switzerland	-0.3	4.0	-3.4	-1.1	-0.5
Jura	-1.1	0.5	**-6.6**	0.9	-1.6
Ticino	-0.1	-1.7	1.4	-2.5	-3.4
Valais	-0.7	-1.3	-0.3	-2.3	-3.3

Table 4.5: Trends [%/decade] of the seasonal and yearly maximum of IVT (upper rows), TPW (middle rows) and steering wind (lower rows) for each region and each season. The trends are calculated from 1979 to 2011. Bold values are statistically significant trends at the 5% significance level for two-sided tests.

in the northern Alpine regions (Prealps, Eastern Switzerland, Jura) and negative in southern Alpine regions (Ticino, Valais). Trends are only statistically significant trends in the Prealps and Valais for autumn. The trends of the yearly maximum of IVT are negative in all regions but are not statistically significant.

The seasonal maximum of TPW features positive trends in all regions and seasons, except for winter when the trend is about zero in Ticino and negative in the remaining four regions. There are statistically significant trends for spring (Prealps, Ticino, Valais) and for summer (Prealps, Valais). The yearly maximum of TPW show positive

trends in all regions. However, no trend of the yearly maximum of TPW is statistically significant.

The trends of the seasonal maximum of steering wind are all negative, except in the northern Alpine regions for summer, in Ticino for autumn and in Jura for winter. The trends of the yearly maximum of steering wind are negative in all regions but they are not statistically significant. The only statistically significant trend is found in Jura for autumn.

4.2.3.2 20CR

Table 4.6 shows the trends of the yearly mean, the yearly 90% quantile and the yearly maximum of IVT, TPW and steering wind using 20CR data.

Trends of the mean

The yearly mean of IVT features a positive trends in the Alps and Southern Alps but the trend is only statistically significant in the Southern Alps. The trend is about zero in Jura. In Eastern Switzerland, the trend is negative and statistically significant. For the TPW, the yearly mean features only negative trends, with only one statistically significant trend for Eastern Switzerland. Unlike the trends of the yearly mean of TPW, the yearly mean of steering wind features one trend of about zero and three positive trends, with statistically significant trends for the Alps and Southern Alps.

Trends of the 90% quantile

The yearly 90% quantile of IVT show the same trends as the yearly mean of IVT, with positive trends in the Alps, Jura and Southern Alps and a negative trend in Eastern Switzerland. However, no trend is statistically significant. The yearly 90% quantile of TPW shows only positive trends in all regions which is the opposite of the trends of the yearly mean of of TPW. The yearly 90% quantile of steering wind features also only positive trends, with three statistically significant trends for the Alps, Jura and Southern Alps.

Trends of the maximum

The yearly maximum of IVT, TPW and steering wind show exclusively positive trends, except for the yearly maximum of IVT in the Alps where the trend is about zero. All trends of the yearly maximum of TPW are statistically significant, while only one trend

of the yearly maximum of IVT is statistically significant, namely in Jura. Finally, the trends of the yearly maximum of steering wind are statistically significant in the Alps and Southern Alps.

Trends [%/decade]	**IVT**	**TPW**	**Steering wind**
Mean			
Alps	0.1	-0.1	**0.3**
Eastern Switzerland	**-0.4**	**-0.3**	0.0
Jura	0.0	-0.1	0.2
Southern Alps	**0.4**	-0.1	**0.5**
90% quantile			
Alps	0.1	0.1	**0.4**
Eastern Switzerland	-0.2	0.1	0.2
Jura	0.2	0.1	**0.6**
Southern Alps	0.3	0.2	**0.4**
Maximum			
Alps	0.0	**0.7**	**0.4**
Eastern Switzerland	0.2	**0.9**	0.1
Jura	**0.7**	**0.9**	0.4
Southern Alps	0.4	**0.4**	**0.6**

Table 4.6: Trends [%/decade] of the yearly mean (upper rows), the yearly 90% quantile (middle rows) and the yearly maximum (lower rows) of IVT, TPW and steering wind for each region. The trends are calculated from 1871 to 2010. Bold values are statistically significant trends at the 5% significance level for two-sided tests.

Chapter 5

Discussion

According to the structure of the presented results, the discussion is equally presented in two parts. The first part discusses the results of the climatological characteristics of IVT, TPW, steering wind and moisture flux. The second part discusses the temporal variability of IVT, TPW and steering wind.

5.1 Climatological characteristics

5.1.1 IVT direction and intensity

The results show that the intensity of daily mean IVT strongly depends on the direction of the flow and differs between the northern (Prealps, Eastern Switzerland, Jura) and southern (Ticino, Valais) Alpine regions. In the northern Alpine regions, the most intense IVTs are most common for westerly south-westerly flow (Figure 4.3a). In addition, the north-easterly flow also contributes to the most intense IVTs. This shows that flows parallel to the topography correspond to the most intense IVTs in the northern Alpine regions. In the southern Alpine regions, flows from the West, South-West and South conrtibute mainly to the most intense IVTs (Figure 4.3b).

Different frequency patterns of IVT's origin can be identified between the northern and southern Alpine regions. These patterns resemble the patterns of the most intense IVTs. South-westersterly and westerly IVTs are most frequent for northern Alpine regions (Figure 4.3a), while north-westerly, westerly and south-westerly IVTs are most frequent for southern Alpine regions (Figure 4.3b). The frequency of southerly IVTs is slighlty lower but important for more intense IVTs, as mentioned above. The distinct differences of frequency and intensity of southerly IVTs between northern and southern Alpine regions show that even the smoothed Alpine orography of the ERA-Interim model can act as a barrier for the moisture sources. This is similar to the findings of Sodemann and Zubler (2010) which found differences of moisture sources of northern

and southern Alpine regions with ERA-40 data.

We found that the most intense IVTs occur in summer and autumn (Table 4.1). As mentioned previously, the directions of the most frequent IVTs are also important for the most intense IVTs. Summer and autumn exhibit a higher percentage of IVTs coming from these directions compared to the other seasons. The frequency of north-easterly IVTs is lower in summer compared to the other seasons. However, the summer is the season which exhibits the most intense IVTs coming from the North-East (Figure 4.1). It is conceivable that these intense IVTs coming from the North-East have their moisture source in the Mediterranean Sea and the moisture is then transported around the Alps (Petrow et al., 2007; Mudelsee et al., 2004). We hypothesise that this transport is caused by a Vb weather situation which is characterised by a low pressure system in the Adriatic region and consequently leads to a cyclonic flow around the Alps (Beurton and Thieken, 2009; Mudelsee et al., 2004).

Interestingly, the intensity of IVTs differs between the regions. The main reason presents probably the difference of the surface pressure between the regions. The surface pressure indicates the level of the region. Thus, the lower the surface pressure the higher the region is located in altitude. Table 5.1 shows the mean surface pressure, the 95% quantile and the maximum of IVT calculated over the whole ERA-Interim time period for each region. The 95% quantile and the maximum of IVT are much higher for Eastern Switzerland and Jura compared to the other regions, since they are located higher and thus have lower mean surface pressure. This shows that there is already a loss of moisture due to the topography before it is vertically integrated.

5.1.2 Yearly cycles

The yearly cycles of IVT, TPW and steering wind show that the yearly cycle of IVT is similar to that of TPW. July and February are the months when the monthly mean of

	Mean surface pressure [hPa]	**95% quantile of IVT [$\mathbf{kg\,m^{-1}s^{-1}}$]**	**Maximum of IVT [$\mathbf{kg\,m^{-1}s^{-1}}$]**
Prealps	890	225	483
Eastern Switzerland	950	311	751
Jura	960	321	688
Ticino	890	174	448
Valais	850	165	361

Table 5.1: Mean surface pressure, 95% quantile and maximum of IVT are calculated over the whole ERA-Interim time period (1979-2011) for the different regions.

IVT is highest and lowest respectively. This is found in all regions except for Eastern Switzerland, where April exhibits the lowest monthly mean of IVT. This is similar for TPW, where the monthly mean of TPW is highest and lowest in the months of August and February respectively. Steering wind shows a different pattern, since December and August are the months in which the monthly mean of steering wind is highest and lowest respectively.

Hence, intense IVTs can be found in all months (Figure 4.4), because the seasonality of TPW and steering wind compensate each other. Furthermore, intense cyclones occur in all seasons (Raible et al., 2008) and can lead to intense IVTs. However, the highest monthly 99% quantile of IVT is found for September and October. These are the months when the TPW exhibits still higher values and the winds get stronger.

5.1.3 Vertical profiles

The vertical profiles of the moisture flux, specific humidity and wind speed show the same seasonal cycle as discussed in the previous section for IVT, TPW and steering wind. The mean moisture flux and mean specific humidity are strongest during sum-

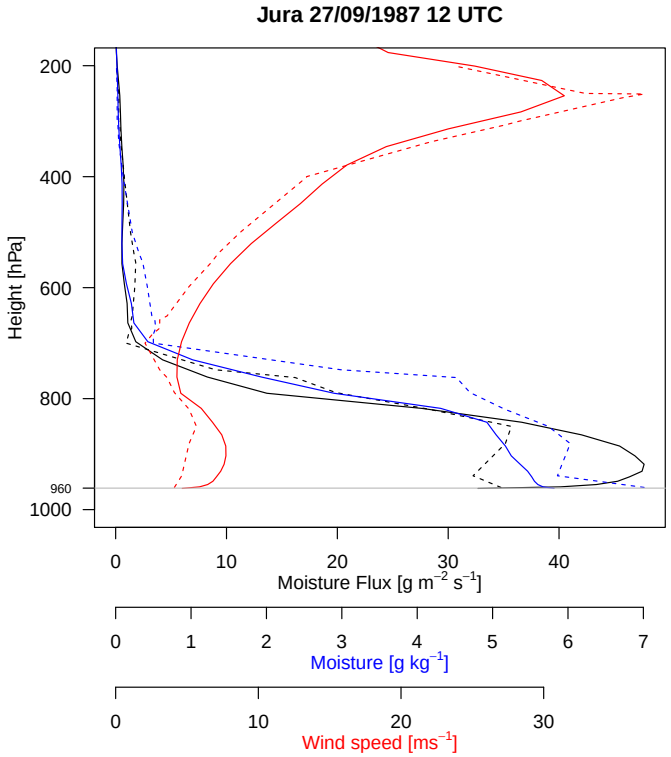

Figure 5.1: Vertical profile of the moisture flux [g m^{-2}s^{-1}] (black), specific humidity [g kg^{-1}] (blue) and wind speed [m s^{-1}] (red) on 27 September 1987 at 12 UTC. The continuous lines show the ERA-Interim data in Jura and the dashed lines show the radio sounding data.

mer throughout the whole vertical profile, whereas the mean wind speed is strongest during winter.

The biggest difference between the northern and southern Alpine regions are the weaker mean moisture fluxes in the southern Alpine regions (Figure 4.7). Comparing the vertical profiles of specific humidity and wind speed (Figure 4.8 and 4.9), we find that the specific humidity is only mildly lower in the southern Alpine regions. However, the wind speed is much lower near the surface in the southern Alpine regions and does not increase with height as fast as in the northern Alpine regions. This could be due to the orographical situation in the southern Alpine regions which leads to the difference between the northern and southern Alpine regions.

The vertical profiles of the seasonal mean of specific humidity show a strong seasonal cycle (Figure 4.8). This is expected due to the temperature dependence of the water vapour capacity of the air. Cooler and thus drier air leads to a higher moist-adiabatic lapse rate which is closer to the dry adiabatic lapse rate (Ambaum, 2010). It can be explained by the fact that a lifted dry air parcel condensates less vapour than a moist air parcel. Condensation of water vapour induces latent heat release which weakens the moist-adiabatic lapse rate (Ambaum, 2010).

Analyses of moisture fluxes on flood days indicate that the intensity at low level is an important factor for flood events (e.g. Figure 5.1). This moist low level jet is forced to ascend due to orography and triggers precipiation (e.g. Martius et al., 2006; Panziera and Germann, 2010). Furthermore, Froidevaux (2014) shows that the direction of moisture flux is crucial. Moisture fluxes perpendicular to the topography are much more effective in triggering floods than fluxes along the topography.

5.2 Temporal variability

5.2.1 Interannual variability

The interannual variability is very distinct for IVT with amplitudes varying between plus and minus 15% (Figure 4.10). The interannual variability of steering wind exhibits almost the same amplitudes as IVT. However, the interannual variability of TPW is less disinct, with amplitudes of about 5 to 10%. Therefore, the explained variance R^2 for the interannual variability of IVT is higher for steering wind than for TPW as a predictor (Table 4.2). However, it is remarkable that the wind on a certain pressure level shows similar or even higher R^2 than steering wind.

The R^2 for the interannual variability of IVT was also calculated with data of North Atlantic Oscillation (NAO) index and El Niño/Southern Oscillation (ENSO) index. However, the R^2 did not reveal any significant correlation between the interannual variability of IVT and the two climate indices. This is similar to the findings of Sodemann and Zubler (2010) who did not find any significant correlation between moisture source variability for Alpine precipitation and the two climate indices. Trenberth et al. (2005) already show that precipitable water is strongly linked with the sea surface temperature variability in the Tropics. Thus, it would be interesting to investigate the correlation between the interannual variability of IVT and the SST variability in the Mediterranean Sea and North Atlantic.

We found that the years of maximal and minimal yearly mean of IVT show distinct differences of the frequencies of IVT direction. The directions from where more intense IVTs come from are more frequent for years of maximal yearly mean of IVT. The directions, which get more frequent, are South-West and West for northern Alpine regions and South-West, West and North-West for southern Alpine regions. The frequencies for these directions increase by 5 to 10% compared to the frequencies of the years of minimal yearly mean of IVT. This implies that the frequency of IVT directions explains to some degree the interannual variability of IVT. Thus, an analysis of the variability of circulation types could help to better understand the interannual variability of IVT.

5.2.2 Wavelet analyses

The wavelet analyses show statistically significant oscillation bands between 5 and 8 years for the standardised yearly mean of IVT in all regions for ERA-Interim data. However, the oscillation bands are only statistically significant in the end of the 20th century for 20CR data. This implies that the oscillation band between 5 and 8 years is not a stable mode in time. The standardised yearly mean of TPW and steering wind exhibit a similar oscillation band as the standardised yearly mean of IVT for

ERA-Interim data. However, the yearly mean of steering wind does not feature this oscillation band between 5 and 8 years in the end of the 20th century for 20CR data.

The standardised yearly mean of IVT of 20CR data shows statistically significant wavelet power in the oscillation band above 32 years. These oscillation bands are visible for all regions. The steering wind also exhibits these oscillation bands. It suggests that the wind is responsible for this periodicity of IVT of more than 32 years. This is in agreement with the results of Welker and Martius (2013). They found that hazardous winds in winter exhibit decadal-scale variability with periods between 36 and 47 years.

Regarding the wavelet analyses of the standardised seasonal mean of IVT, the oscillation bands are visible in all seasons but they are most distinct in autumn. However, this is not the case for the standardised seasonal mean of TPW and steering wind. While the steering wind does not exhibit statistically significant oscillation bands between 5 and 8 years in spring, the same is true for TPW in summer in the southern Alpine regions. The most distinct oscillation bands are featured in spring for TPW and in winter for steering wind. In the other seasons, the oscillation bands are less distinct and occur at different frequencies. However, it seems that TPW is more important for the periodicity of IVT in spring, whereas the steering wind is more important in winter.

5.2.3 Trend analyses

The trend analyses reveal negative trends of the yearly mean, the yearly 90% quantile and the yearly maximum of IVT over the defined regions with ERA-Interim data (Tables 4.3, 4.4 and 4.5). However, no trend is statistically significant. These negative trends are consistent throughout the Alpine region but there are also positive trends in the South-East of the Alpine region around the Gulf of Venice (Figure 5.2).

Comparing the trends of ERA-Interim data with 20CR data, we can find only one negative trend of the yearly mean of IVT with 20 CR data, namely in Eastern Switzerland (Table 4.6). The trends of 20CR and ERA-Interim are contrasting because the trends of yearly mean of steering wind are positive with 20CR data and negative with ERA-Interim data. These trends of steering wind are stronger than the trends of the yearly mean of TPW which are negative with 20CR data and positive with ERA-Interim data. Thus, the trends of steering wind predominate the trends of TPW and determine the trends of IVT for ERA-Interim and 20CR data.

If the trends of the yearly mean of IVT are calculated with 20CR data only for the time period 1979 to 2010, the trends are even more positive than for the whole 20CR time period. However, the trends of the yearly mean of TPW and steering wind are positive and negative respectively. These trends are in contrast to the trends of the whole 20CR time period but they are similar to the trends with ERA-Interim data. In this case, the

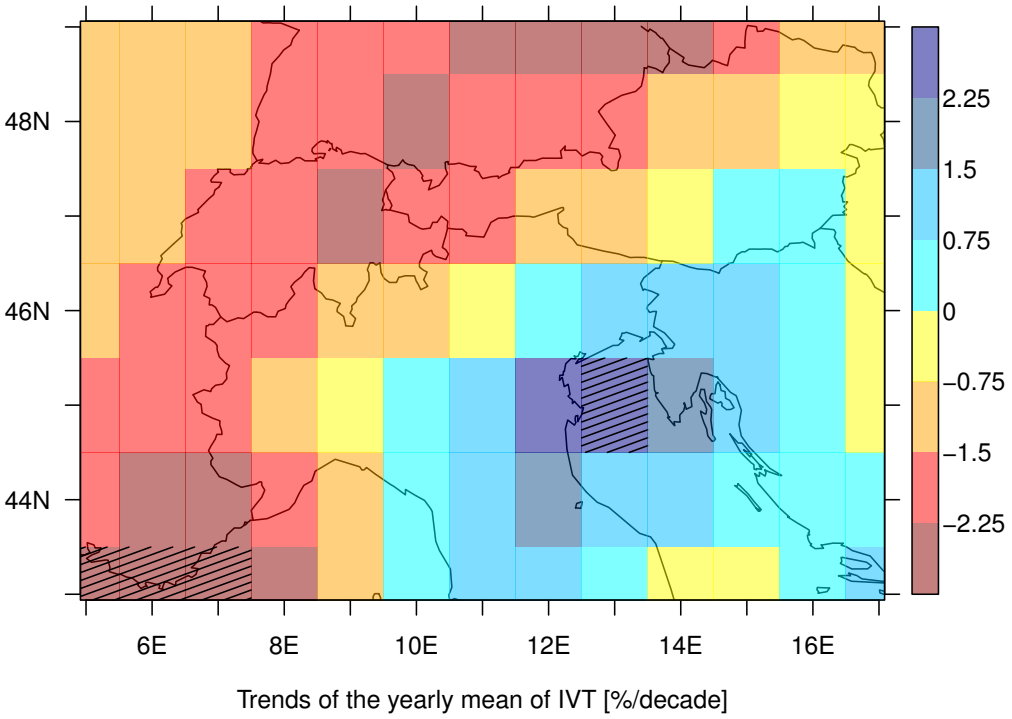

Figure 5.2: Map showing the trends of the yearly mean of IVT [%/decade] for the ERA-Interim time period (1979-2011). The dashed grid boxes show statistically significant trends at the 5% significance level for two-sided tests.

trends of TPW are stronger than the trends of steering wind and lead to these positive trends of the yearly mean of IVT.

The trends of the seasonal mean of IVT are slightly positive in summer for all regions except for Eastern Switzerland. The other seasons reveal negative trends. TPW exhibits positive trends in summer and also in spring for all regions. These trends of the seasonal mean of TPW are in accordance with the findings of Mattar et al. (2011) who used the reanalysis data from National Center of Envirionmental Prediction (NCEP-1) and radio sounding data for their analyses. The trends of the seasonal mean of steering wind exhibit only negative trends except in summer for Jura. These negative trends are stronger in autumn and winter than in spring and summer but only the trends in winter for the southern Alpine regions are statistically significant.

In summary, there are opposing trends of IVT for the different seasons. Furthermore, most of the trends are not statistically significant, including the trends of the 90% quantile and the maximum. Most of the trends of TPW are also not statistically significant. However, the map of the yearly mean of TPW (Figure 5.3) shows that there are several statistically significant trends in the eastern and south-eastern parts of the Alpine region. Regarding the whole of Europe, previous studies have shown that the positive trends of column integrated water vapour over Europe are only small and not statistically significant (Trenberth et al., 2005; Ross and Elliott, 2001). These weak trends

are mostly caused by the fact that reanalysis products suffer from time dependent biases (IPCC, 2013). The trends of steering wind also did not reveal many statistically significant trends although most of the trends are negative. Bett et al. (2013) did also not find any evident trends in wind speed across Europe with 20CR data due to the large decadal variability.

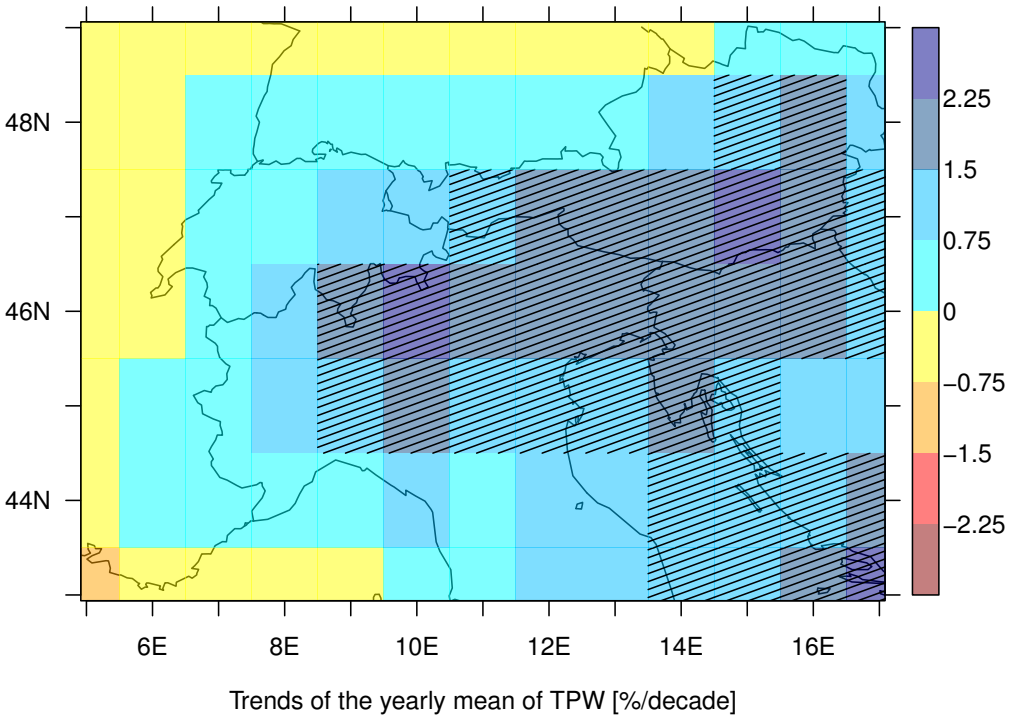

Figure 5.3: Map showing the trends of the yearly mean of TPW [%/decade] for the ERA-Interim time period (1979-2011). The dashed grid boxes show statistically significant trends at the 5% significance level for two-sided tests.

Chapter 6

Conclusions

Previous studies have assessed the importance of atmospheric rivers for the moisture transport in the extratropics and their contribution to flood events. However, the existing literature lacks a perspective on climatological characteristics and temporal variability of local moisture fluxes. To account for this gap of knowledge, the study at hand investigated the climatological characteristics and the temporal variability of IVT. The analyses were performed for different Alpine regions.

6.1 Summary

The following climatological characteristics were found:

- Daily mean IVT amplitudes strongly depend on the direction of the flow. The northern Alpine regions exhibit two peaks from where the most intense IVTs come. One peak is represented by the IVTs coming from the North-East and the other peak is associated with westerly and south-westerly IVTs. The southern Alpine regions show a less distinct pattern. There, westerly, south-westerly and southerly IVTs are mainly responsible for the most intense IVTs.
- The northern and southern Alpine regions show that the direcitons where the most intense IVTs come from are also the most frequent directions for IVTs. The differences between the seasonal frequency of the IVT direction are about 5 to 10%.
- The most intense IVTs occur in summer and autumn with maximal IVTs of about 600 to 700 $\mathrm{kg\,m^{-1}s^{-1}}$ in northern Alpine regions and 300 to 400 $\mathrm{kg\,m^{-1}s^{-1}}$ in southern Alpine regions. However, weak IVTs are most frequent. In northern Alpine regions about 80% of the IVTs are below 200 $\mathrm{kg\,m^{-1}s^{-1}}$. For the southern Alpine regions, this percentage is around 95%.

- The yearly cycle of IVT shows that the highest monthly mean can be found in July and the lowest in February or April. This is similar to the yearly cycle of TPW, which exhibits the highest monthly mean in August and the lowest in February. In contrast, the yearly cycle of steering wind features the highest monthly mean in December and the lowest in August. The highest monthly 99% quantile of IVT is calculated for September and October. These are the months when the TPW still exhibits higher values and the winds get stronger.

- The vertical profiles show that most intense mean moisture flux occurs in summer. The level that exhibits the strongest intensity of the mean moisture flux is betweem 50 and 100 hPa above the surface level. This is caused by the fact that the wind speed increases with height up to 200 hPa, whereas the specific humdity decreases rapidly with height.

The following characteristics of temporal variability were found:

- The interannual variability of IVT is around 10 to 15%. This interannual variability of IVT is highly correlated with the interannual variability of steering wind. The R^2 is about 0.8 depending on the region. This R^2 is even higher if it is calculated with the wind speed on a specific pressure level, which varies between 750 and 650 hPa depending on the region. The R^2 is clearly lower for TPW, with values around 0.5 for northern Alpine regions and with values below 0.25 for southern Alpine regions.

- The wavelet analyses show that IVT exhibits a periodicty of 5 to 8 years in the end of the 20th century. However, it is not possible to ascribe the periodicty of IVT to the periodicty of TPW or steering wind because both of them feature also a periodicity of 5 to 8 years. IVT shows also a decadal-scale variability with periods of more than 36 years. This periodicity can be ascribed to the steering wind which also exhibits a periodicity of more than 36 years.

- The trends of the yearly mean, the yearly 90% quantile and the yearly maximum of IVT are all negative over Switzerland with ERA-Interim data. The trends of the seasonal mean of IVT are positive in summer in 4 of 5 regions and negative in all other seasons. However, no trend is statistically significant. The trends of TPW and steering wind are in most of the cases contrary because TPW exhibits positive trends, whereas steering wind shows negative trends. This implies that the trends of steering wind predominate the trends of TPW and determine the negative trends of IVT. However, most of the trends of TPW and steering wind are also not statistically significant which is in accordance with other studies.

6.2 Outlook

In this last section, some open issues are shortly discussed and therefore possible research topics are presented.

The interannual variability of IVT is not fully understood. Thus, the following points should be further elucidated. As mentioned in the discussion chapter, the interannual variability of IVT could be correlated with the SST variability in the Mediterranean Sea and North Atlantic. Furthermore, the investigation of the frequency of circulation types presents an additional point which could increase the comprehension of the interannual variability of IVT.

The wavelet analyses reveal some remarkable patterns of the periodicity of IVT. However, the analyses are largely descriptive. Thus, subsequent research should focus on the reasons for the periodicity of IVT. Furthermore, expanding these analyses over the whole of Europe would already show if the periodicity is detectable also in a wider area or if it is a small-scale phenomena.

Appendix

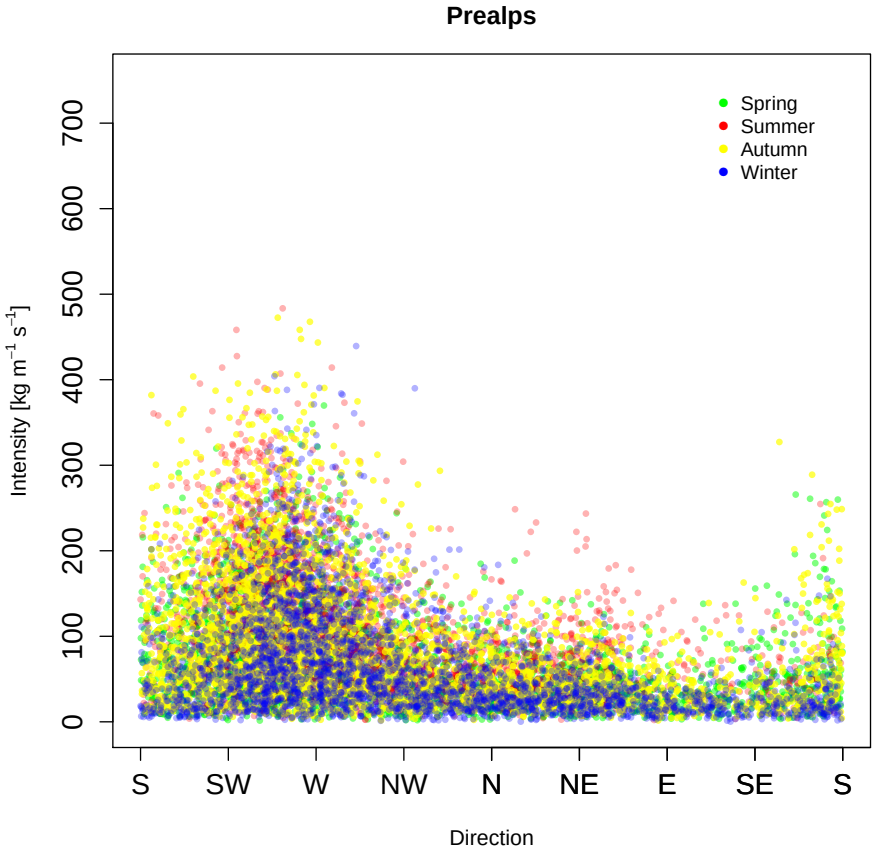

Figure A.1: Daily mean IVTs of the Prealps. The abscissa represents the IVT direction and the oridnate the IVT intensity [kg m^{-1}s^{-1}]. All days of the ERA-Interim time period (1979-2011) are shown with green, red, yellow and blue dots for the days in spring, summer, autumn and winter.

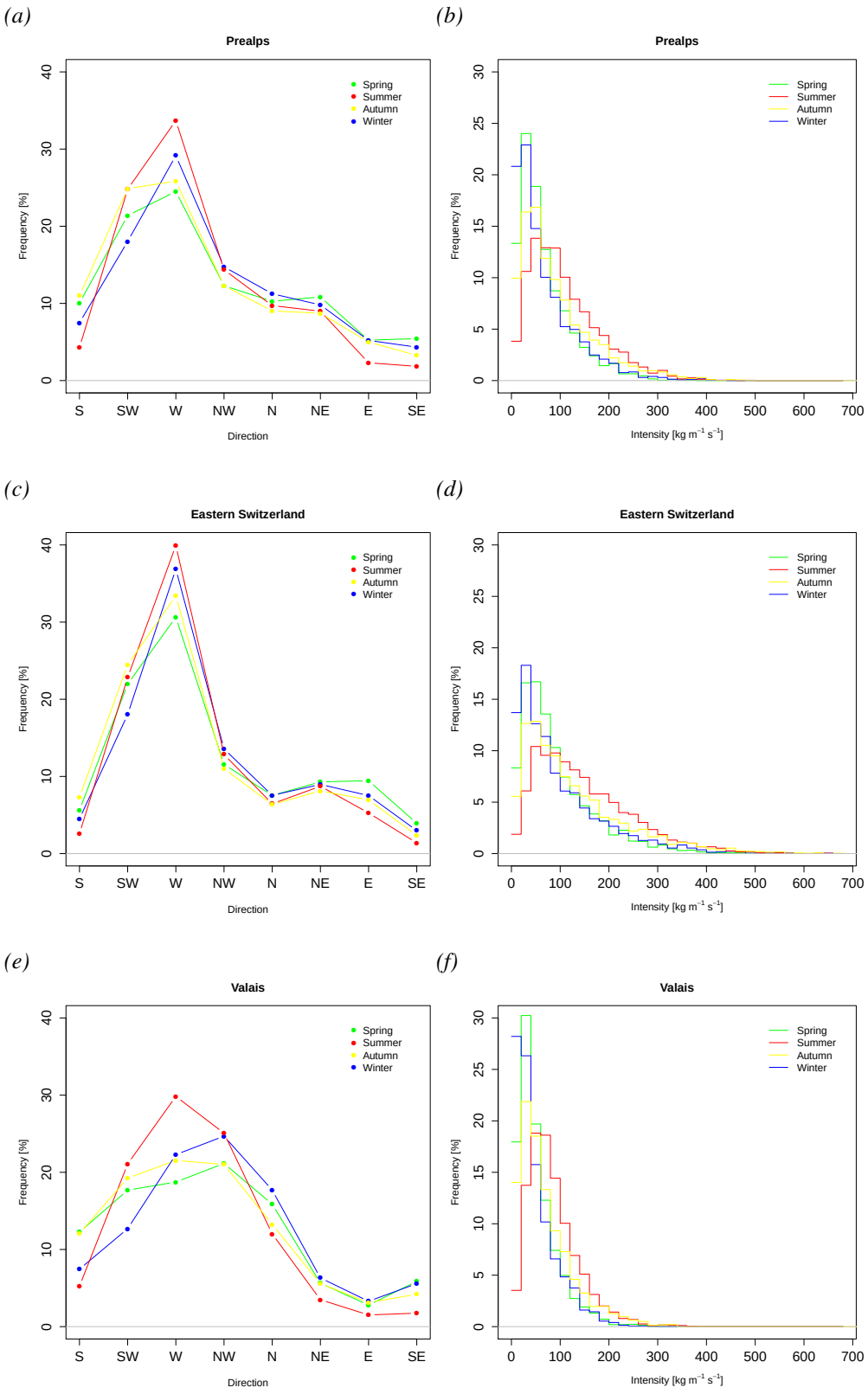

Figure A.2: Left column: relative frequency of IVT direction for each 45° sector (e.g. S = 157.5°-202.5°). Right column: relative frequency of IVT intensity for each class of 20 kg m^{-1}s^{-1}. Daily mean IVTs of the ERA-Interim time period (1979-2011) are included. The colors indicate the different seasons (green = spring, red = summer, yellow = autumn, blue = winter). The plots are shown for the Prealps (upper row), Eastern Switzerland (middle row) and Valais (lower row).

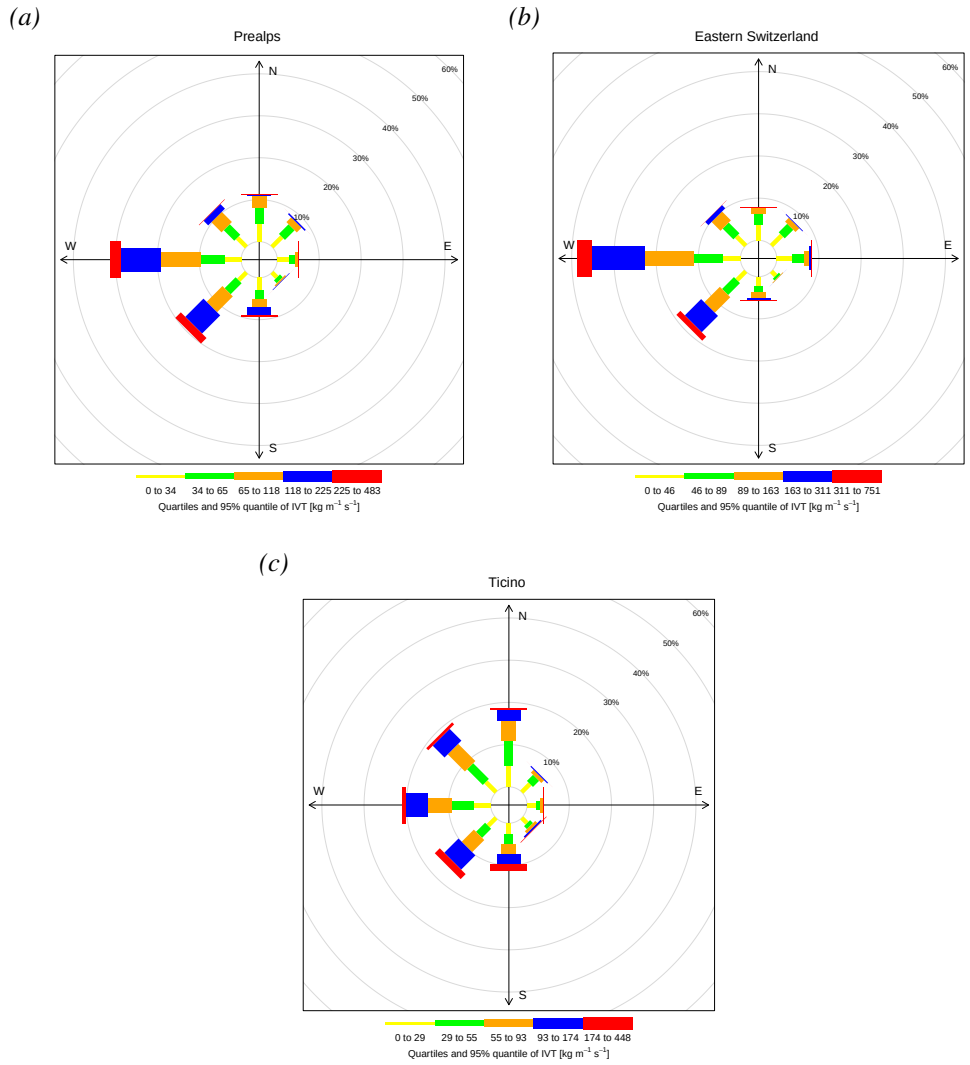

Figure A.3: Wind rose plots representing the relative frequency of IVT direction for each 45° sector (e.g. S = 157.5°-202.5°) for the Prealps (a), Eastern Switzerland (b) and Valais (c). Daily mean IVTs of the ERA-Interim time period (1979-2011) are included. The colors indicate different quantile limits (yellow = 0-25%, green = 25-50%, orange = 50-75%, blue = 75-95%, red = 95-100%) and their percentage for each 45° sector.

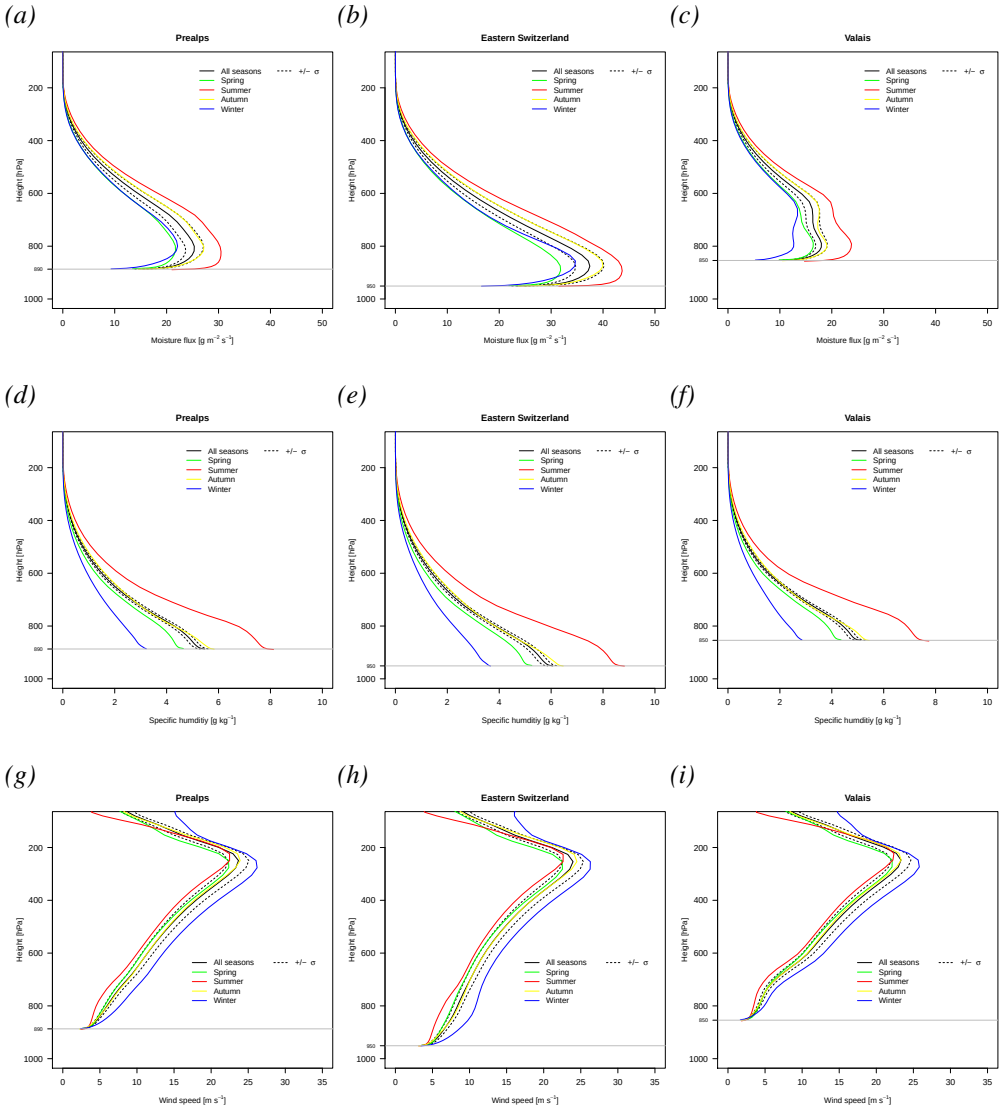

Figure A.4: Mean vertical profile of the moisture flux [g m^{-2}s^{-1}] (upper row), specific humidity [g kg^{-1}] (middle row) and wind speed [m s^{-1}] (lower row) at 12 UTC including all days of the ERA-Interim time period (1979-2011). The colors of the lines indicate the seasons with green, red, yellow and blue indicating the mean intensity in spring, summer, autmn and winter. The black line shows the mean over all seasons and the dashed black lines limit the range from plus to minus one standard deviation from the yearly means. The vertical profiles are shown for the Prealps (left column), Eastern Switzerland (middle column) and Ticino (right column).

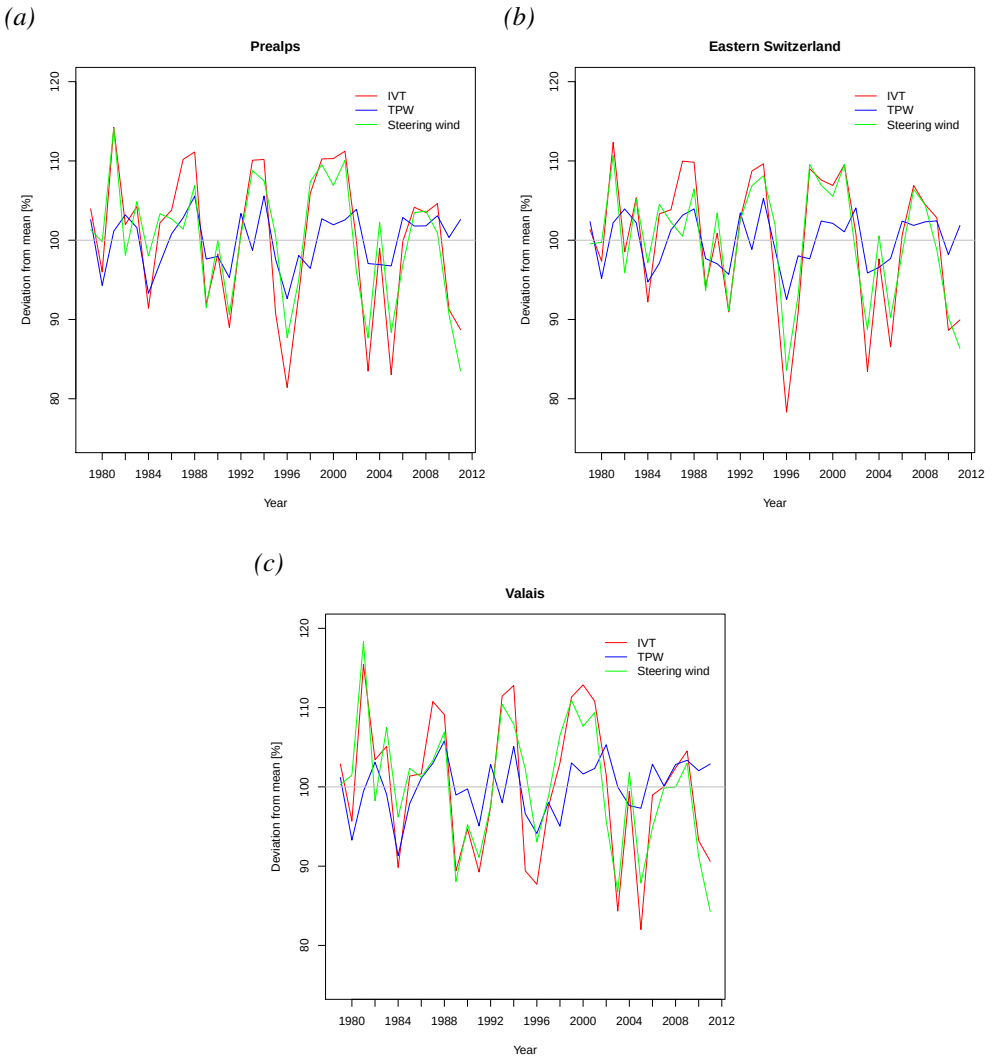

Figure A.5: Yearly mean of IVT, TPW and steering wind are shown as relative deviation from the long-term mean of the ERA-Interim time period (1979-2011) in the Prealps (a), Eastern Switzerland (b) and Valais (c). The red, blue and green line show the yearly mean of IVT, TPW and steering wind.

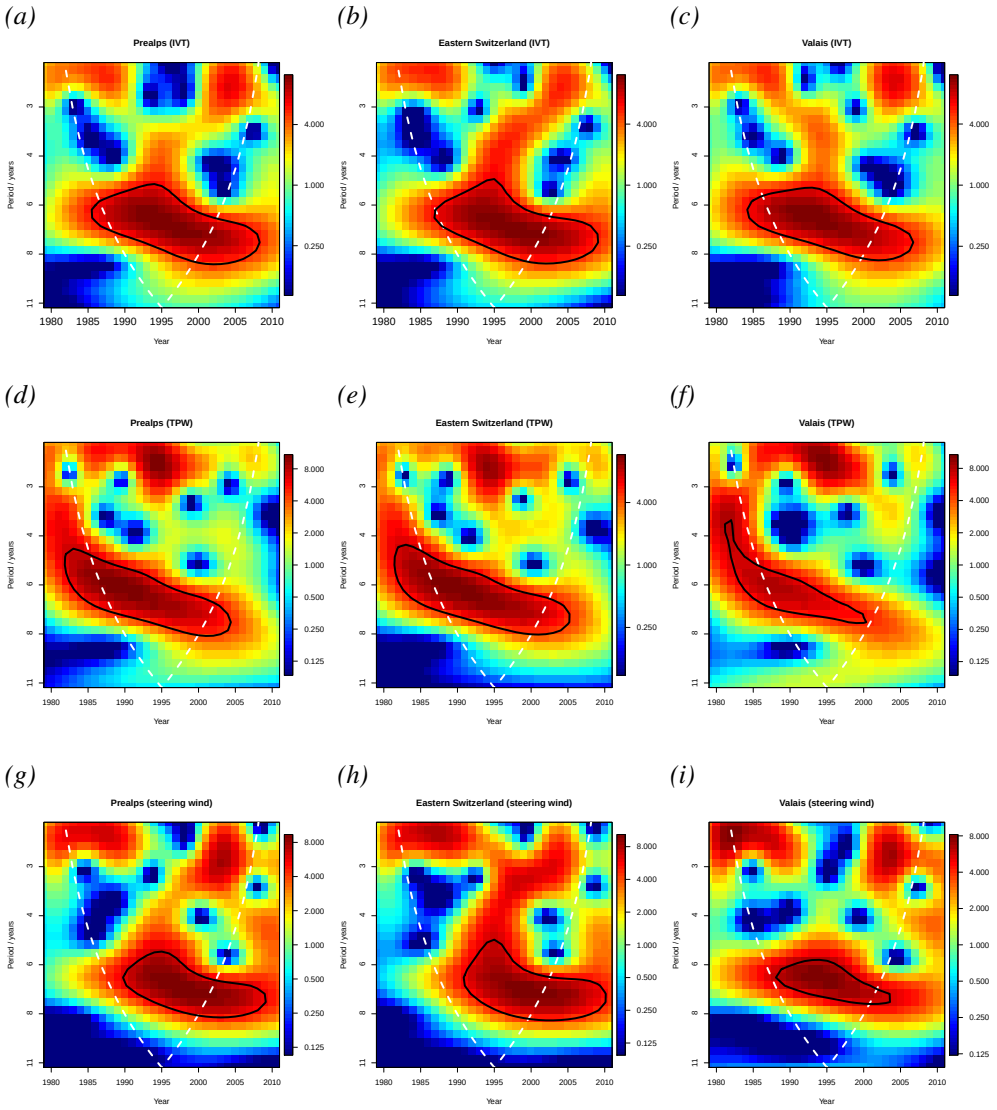

Figure A.6: CWT power spectra of the standardized yearly mean of IVT (upper row), TPW (middle row) and steering wind (lower row) in the Prealps (left column), Eastern Switzerland (middle column) and Valais (right column) for the ERA-Interim time period (1979-2011). The abscissa indicates the time and the ordinate features the period in years. The black contour lines show the 5% significance level. The dashed white line denotes the COI where edge effects become important.

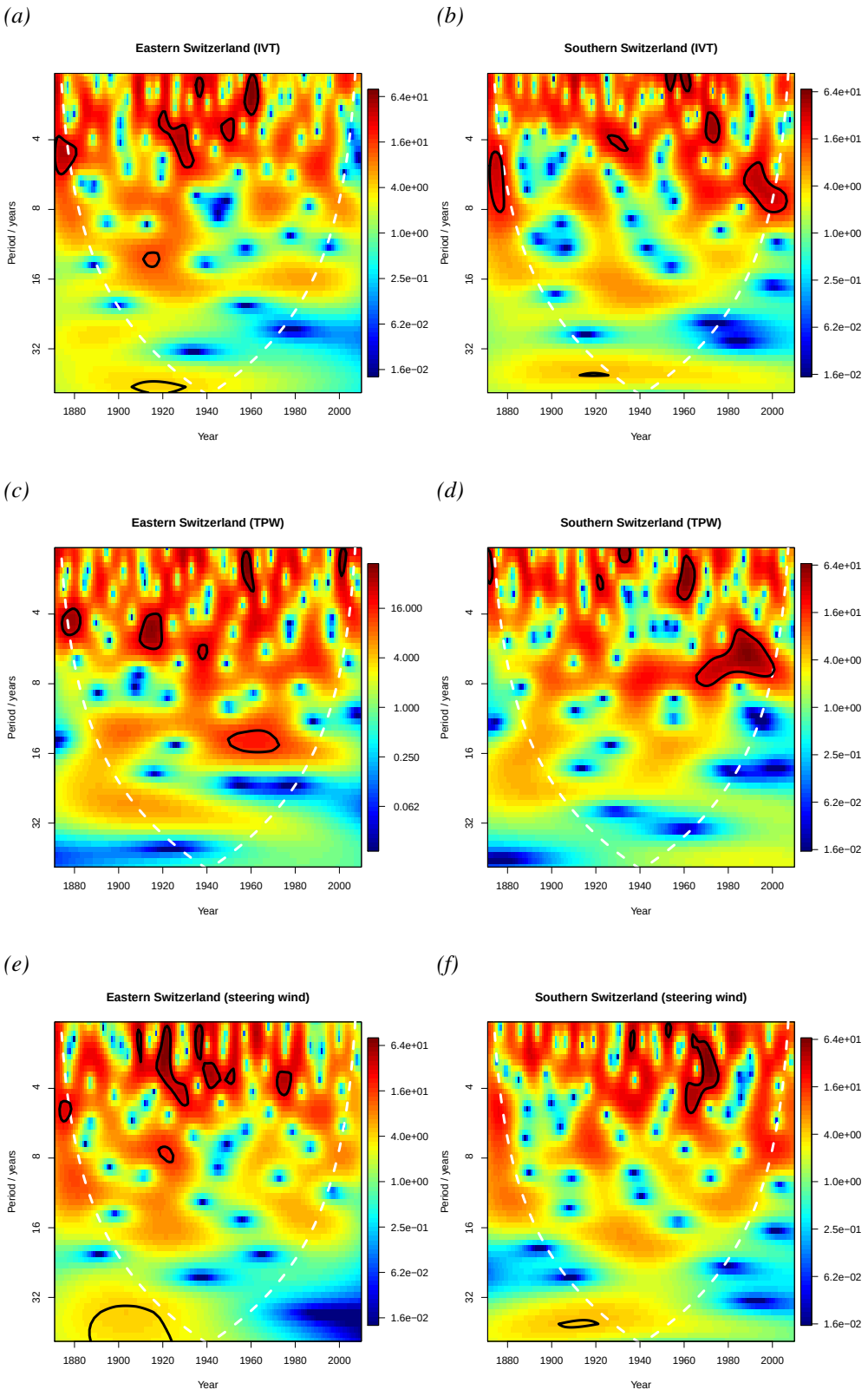

Figure A.7: CWT power spectra of the standardized yearly mean of IVT (upper row), TPW (middle row) and steering wind (lower row) in Eastern Switzerland (left column) and Southern Alps (right column) for the 20CR time period (1871-2010). The abscissa indicates the time and the ordinate features the period in years. The black contour lines show the 5% significance level. The dashed white line denotes the COI where edge effects become important.

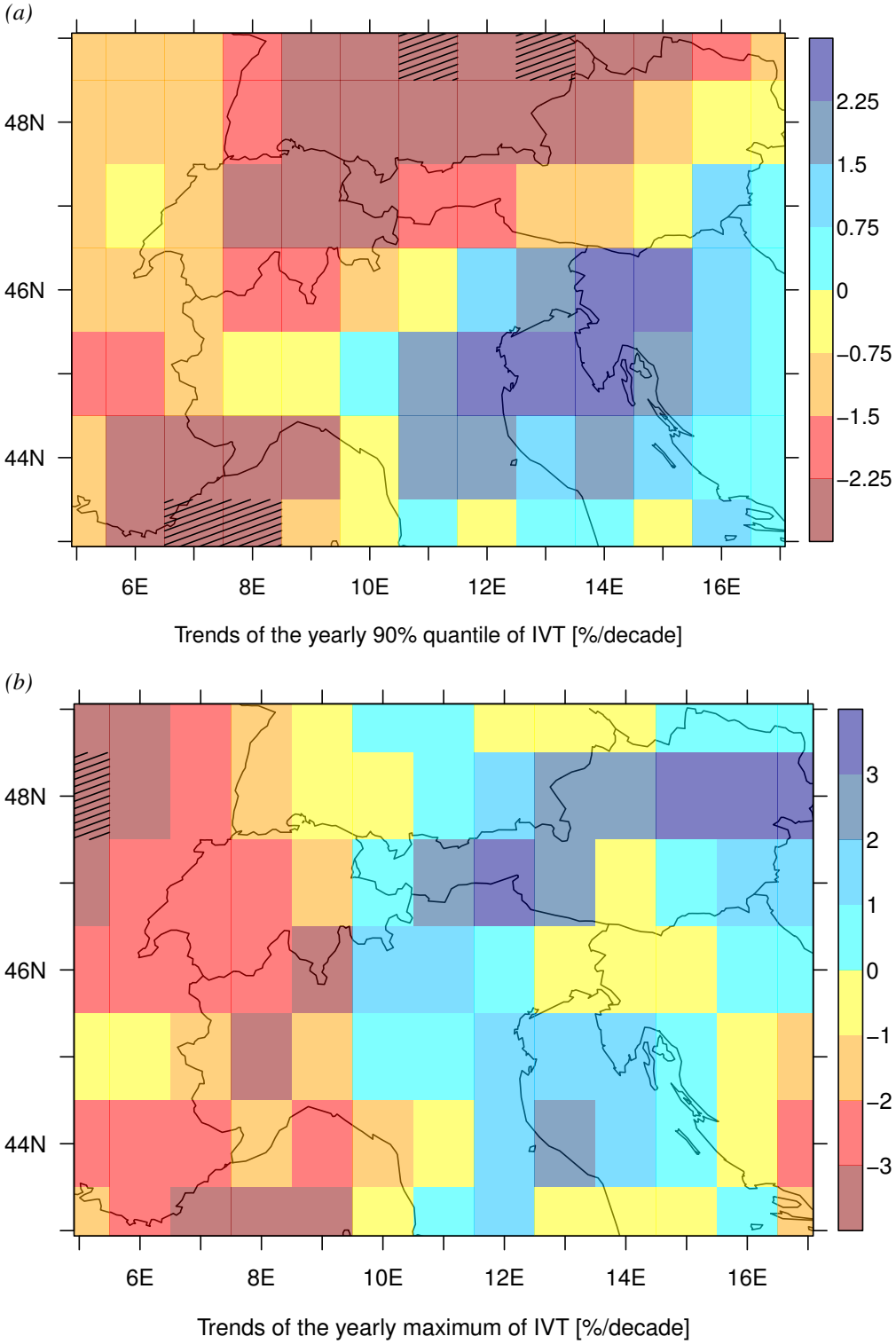

Figure A.8: Map showing the trends of the yearly 90% quantile (a) and the yearly maximum (b) of IVT [%/decade] for the ERA-Interim time period (1979-2011). The dashed grid boxes show statistically significant trends at the 5% significance level for two-sided tests.

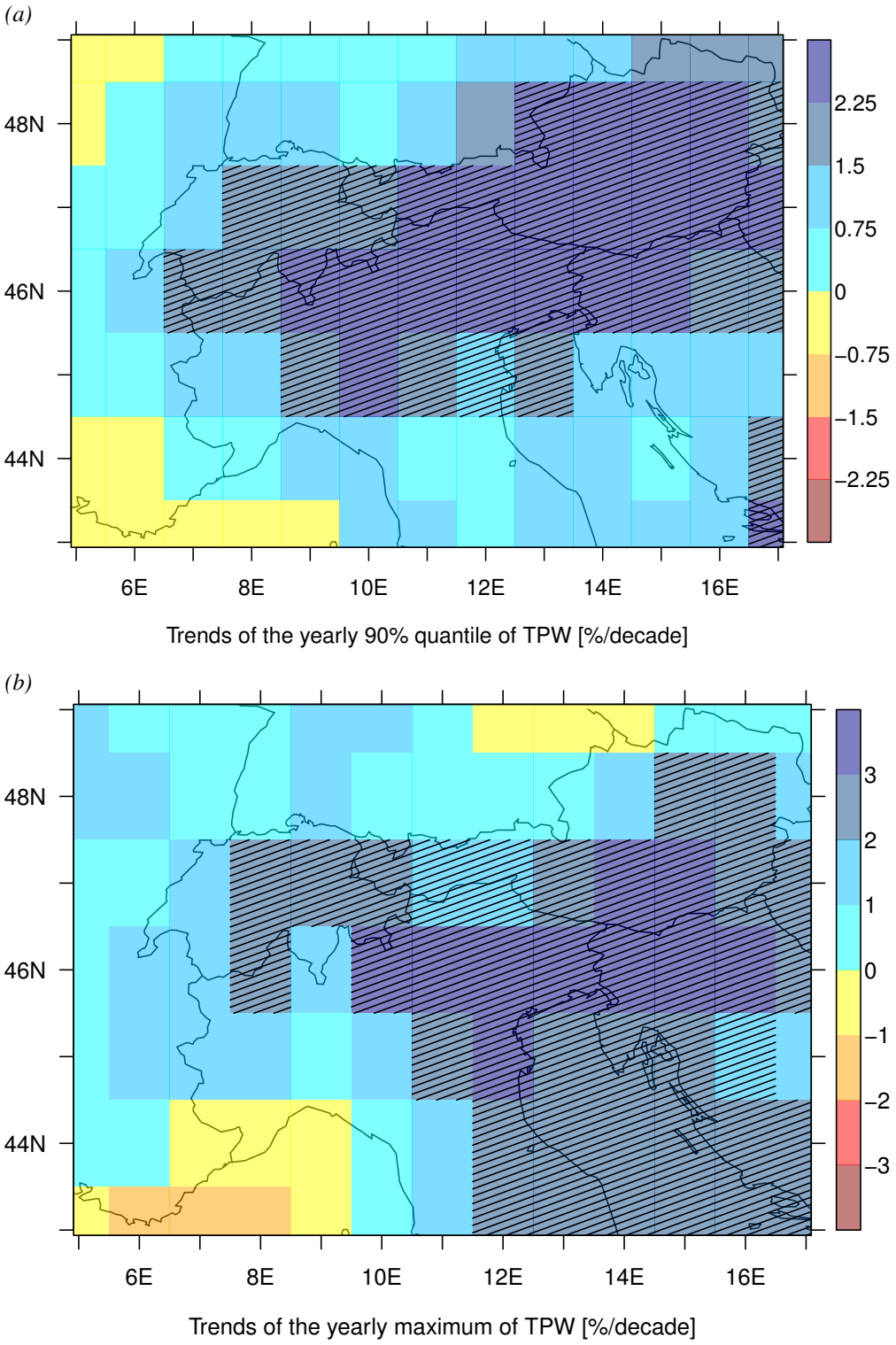

Figure A.9: Map showing the trends of the yearly 90% quantile (a) and the yearly maximum (b) of TPW [%/decade] for the ERA-Interim time period (1979-2011). The dashed grid boxes show statistically significant trends at the 5% significance level for two-sided tests.

List of Figures

List of Tables

Bibliography

Ambaum, M. H. P. 2010. *Thermal Physics of the Atmosphere. Advancing Weather and Climate Science*. Wiley-Blackwell.

Bett, P. E., H. E. Thornton, and R. T. Clark. 2013. European wind variability over 140 yr. *Advances in Science and Research* **10**, 51–58.

Beurton, S., and A. H. Thieken. 2009. Seasonality of floods in Germany. *Hydrological Sciences Journal* **54**, 62–76.

CH2011 2011. Swiss Climate Change Scenarios CH2011. *published by C2SM, MeteoSwiss, ETH, NCCR Climate, and OcCC, Zurich, Switzerland, 88pp*.

Compo, G. P., J. S. Whitaker, P. D. Sardeshmukh, N. Matsui, R. J. Allan, X. Yin, B. E. Gleason, R. S. Vose, G. Rutledge, P. Bessemoulin, S. Brönnimann, M. Brunet, R. I. Crouthamel, A. N. Grant, P. Y. Groisman, P. D. Jones, M. C. Kruk, A. C. Kruger, G. J. Marshall, M. Maugeri, H. Y. Mok, Ø. Nordli, T. F. Ross, R. M. Trigo, X. L. Wang, S. D. Woodruff, and S. J. Worley. 2011. The Twentieth Century Reanalysis Project. *Quarterly Journal of the Royal Meteorological Society* **137**, 1–28.

Dee, D., J. Fasullo, D. Shea, and J. Walsh. 2014. The Climate Data Guide: Atmospheric Reanalysis: Overview & Comparison Tables. Accessed on 9 April 2014, https://climatedataguide.ucar.edu/climate-data/atmospheric-reanalysis-overview-comparison-tables.

Dee, D. P., S. M. Uppala, A. J. Simmons, P. Berrisford, P. Poli, S. Kobayashi, U. Andrae, M. A. Balmaseda, G. Balsamo, P. Bauer, P. Bechtold, A. C. M. Beljaars, L. van de Berg, J. Bidlot, N. Bormann, C. Delsol, R. Dragani, M. Fuentes, A. J. Geer, L. Haimberger, S. B. Healy, H. Hersbach, E. V. Hólm, L. Isaksen, P. Kållberg, M. Köhler, M. Matricardi, A. P. McNally, B. M. Monge-Sanz, J.-J. Morcrette, B.-K. Park, C. Peubey, P. de Rosnay, C. Tavolato, J.-N. Thépaut, and F. Vitart. 2011. The Era-Interim reanalysis: configuration and performance of the data assimilation system. *Quarterly Journal of the Royal Meteorological Society* **137**, 553–597.

FOEN 2008. Hochwasser 2005 in der Schweiz, Synthesebericht zur Ereignisanalyse. Available online at, http://www.bafu.admin.ch/publikationen/publikation/00819/index.html?lang=de.

FOEN 2014. Extremereignisse. Accessed on 24 April 2014, http://www.bafu.admin.ch/hydrologie/01834/02041/index.html?lang=de.

Froidevaux, P. 2014. *Atmospheric precursors to flood events*. PhD thesis. University of Bern.

Grinsted, A., J. C. Moore, and S. Jevrejeva. 2004. Application of the cross wavelet transform and wavelet coherence to geophysical time series. *Nonlinear Processes in Geophysics* **11**, 561–566.

Held, I. M., and B. J. Soden. 2006. Robust Responses of the Hydrological Cycle to Global Warming. *Journal of Climate* **19**, 5686–5699.

Hilker, N., A. Badoux, and C. Hegg. 2009. The Swiss flood and landslide damage database 1972-2007. *Natural Hazards and Earth System Sciences* **9**, 913–925.

IPCC 2013. *Climate Change 2013: The Physical Science Basis. Contribution of Working Group I to the Fifth Assessment Report of the Intergovernmental Panel on Climate Change*. [Stocker, T.F., D. Qin, G.-K. Plattner, M. Tignor, S.K. Allen, J. Boschung, A. Nauels, Y. Xia, V. Bex and P.M. Midgley (eds.)]. Cambridge University Press, Cambridge, United Kingdom and New York, NY, USA, 1535 pp.

Lavers, D. A., and G. Villarini. 2013. The nexus between atmospheric rivers and extreme precipitation across Europe. *Geophysical Research Letters* **40**, 3259–3264.

Lavers, D. A., G. Villarini, R. P. Allan, E. F. Wood, and A. J. Wade. 2012. The detection of atmospheric rivers in atmospheric reanalyses and their links to British winter floods and the large-scale climatic circulation. *Journal of Geophysical Research: Atmospheres* **117**, n/a–n/a.

Lavers, D. A., R. P. Allan, E. F. Wood, G. Villarini, D. J. Brayshaw, and A. J. Wade. 2011. Winter floods in Britain are connected to atmospheric rivers. *Geophysical Research Letters* **38**, n/a–n/a.

Martius, O., E. Zenklusen, C. Schwierz, and H. C. Davies. 2006. Episodes of alpine heavy precipitation with an overlying elongated stratospheric intrusion: a climatology. *International Journal of Climatology* **26**, 1149–1164.

Mattar, C., J. A. Sobrino, Y. Julien, and L. Morales. 2011. Trends in column integrated water vapour over europe from 1973 to 2003. *International Journal of Climatology* **31**, 1749–1757.

Mudelsee, M., M. Börngen, G. Tetzlaff, and U. Grünewald. 2004. Extreme floods in central Europe over the past 500 years: Role of cyclone pathway "'Zugstrasse Vb"'. *Journal of Geophysical Research: Atmospheres* **109**, D23101.

Neiman, P. J., F. M. Ralph, G. A. Wick, J. D. Lundquist, and M. D. Dettinger. 2008. Meteorological Characteristics and Overland Precipitation Impacts of Atmospheric Rivers Affecting the West Coast of North America Based on Eight Years of SSM/I Satellite Observations. *Journal of Hydrometeorology* **9**, 22–47.

Neiman, P. J., L. J. Schick, F. M. Ralph, M. Hughes, and G. A. Wick. 2011. Flooding in Western Washington: The Connection to Atmospheric Rivers*. *Journal of Hydrometeorology* **12**, 1337–1358.

Oki, T., and S. Kanae. 2006. Global hydrological cycles and world water resources. *Science* **313**, 1068–1072.

Panziera, L., and U. Germann. 2010. The relation between airflow and orographic precipitation on the southern side of the Alps as revealed by weather radar. *Quarterly Journal of the Royal Meteorological Society* **136**, 222–238.

Petrow, T., B. Merz, K.-E. Lindenschmidt, and A. H. Thieken. 2007. Aspects of seasonality and flood generating circulation patterns in a mountainous catchment in south-eastern Germany. *Hydrology and Earth System Sciences* **11**, 1455–1468.

Raible, C. C., P. M. Della-Marta, C. Schwierz, H. Wernli, and R. Blender. 2008. Northern Hemisphere Extratropical Cyclones: A Comparison of Detection and Tracking Methods and Different Reanalyses. *Monthly Weather Review* **136**, 880–897.

Ralph, F. M., and M. D. Dettinger. 2011. Storms, floods, and the science of atmospheric rivers. *Eos, Transactions American Geophysical Union* **92**, 265–266.

Ralph, F. M., P. J. Neiman, G. A. Wick, S. I. Gutman, M. D. Dettinger, D. R. Cayan, and A. B. White. 2006. Flooding on California's Russian River: Role of atmospheric rivers. *Geophysical Research Letters* **33**, n/a–n/a.

Ross, R. J., and W. P. Elliott. 2001. Radiosonde-based northern hemisphere tropospheric water vapor trends. *Journal of Climate* **14**, 1602–1612.

Rössler, O., P. Froidevaux, U. Börst, R. Rickli, O. Martius, and R. Weingartner. 2014. Retrospective analysis of a nonforecasted rain-on-snow flood in the Alps - a matter of model limitations or unpredictable nature?. *Hydrology and Earth System Sciences* **18**, 2265–2285.

Sodemann, H., and E. Zubler. 2010. Seasonal and inter-annual variability of the moisture sources for Alpine precipitation during 1995–2002. *International Journal of Climatology* **30**, 947–961.

Stucki, P., R. Rickli, S. Brönnimann, O. Martius, H. Wanner, D. Grebner, and J. Luterbacher. 2012. Weather patterns and hydro-climatological precursors of extreme floods in Switzerland since 1868. *Meteorologische Zeitschrift* **21**, 531–550.

Torrence, C., and G. P. Compo. 1998. A practical guide to Wavelet Analysis. *Bulletin of the American Meteorological Society* **79**, 61–78.

Trenberth, K. E., J. Fasullo, and L. Smith. 2005. Trends and variability in column-integrated atmospheric water vapor. *Climate Dynamics* **24**, 741–758.

Welker, C., and O. Martius. 2013. Decadal-scale variability in hazardous winds in northern Switzerland since end of the 19th century. *Atmospheric Science Letters*.

Acknowledgements

I would like to say a big thank you to Olivia Romppainen-Martius and Paul Froidevaux for supervising my work and giving me the opportunity to write the thesis in this interesting field of research. Their support and knowledge helped me a lot to write this thesis. They always took time to discuss my questions or to give inputs.

Great thanks go to Christoph Welker for his advices and explanations. Further, a big thank goes to Andrey Martynov and Marco Rohrer who solved and answered any of my IT problems and questions. I also thank my fellow students Matthias Röthlisberger and Valérie Fazan for their corrrections and inputs. Furthermore, I am greatly thankful Verena Huber for her great help as proofreader. Finally, I would like to thank my family and Corinne for their great support and encouragement throughout my studies.

Declaration

under Art. 28 Para. 2 RSL 05

Last, first name:	Berger, Donatus
Matriculation number:	09-203-167
Programme:	M.Sc. in Climate Sciences
	Bachelor ☐ Master ☒ Dissertation ☐
Thesis title:	Moisture Fluxes over the Alps
Thesis supervisor:	Prof. Dr. Olivia Romppainen-Martius

I hereby declare that this submission is my own work and that, to the best of my knowledge and belief, it contains no material previously published or written by another person, except where due acknowledgement has been made in the text. In accordance with academic rules and ethical conduct, I have fully cited and referenced all material and results that are not original to this work. I am well aware of the fact that, on the basis of Article 36 Paragraph 1 Letter o of the University Law of 5 September 1996, the Senate is entitled to deny the title awarded on the basis of this work if proven otherwise.

Bern, September 12, 2014